

RESEARCH ARTICLE

Tek (Tie2) is not required for cardiovascular development in zebrafish

Zhen Jiang^{1,2,*}, Claudia Carlantoni^{1,2}, Srinivas Allanki^{1,2}, Ingo Ebersberger^{3,4,5,*} and Didier Y. R. Stainier^{1,2,*}

ABSTRACT

Angiopoietin/TIE signalling plays a major role in blood and lymphatic vessel development. In mouse, *Tek* (previously known as *Tie2*) mutants die prenatally due to a severely underdeveloped cardiovascular system. In contrast, in zebrafish, previous studies have reported that although embryos injected with *tek* morpholinos (MOs) exhibit severe vascular defects, *tek* mutants display no obvious vascular malformations. To further investigate the function of zebrafish Tek, we generated a panel of loss-of-function *tek* mutants, including RNA-less alleles, an allele lacking the MO-binding site, an in-frame deletion allele and a premature termination codon-containing allele. Our data show that all these mutants survive to adulthood with no obvious cardiovascular defects. MO injections into *tek* mutants lacking the MO-binding site or the entire *tek* locus cause similar vascular defects to those observed in MO-injected +/- siblings, indicating off-target effects of the MOs. Surprisingly, comprehensive phylogenetic profiling and synteny analyses reveal that *Tek* was lost in the largest teleost clade, suggesting a lineage-specific shift in the function of TEK during vertebrate evolution. Altogether, these data show that Tek is dispensable for zebrafish development, and probably dispensable in most teleost species.

KEY WORDS: *Tek* (*Tie2*), Cardiovascular development, Genome editing, Morpholino, Evolutionary genetics, Functional diversification

INTRODUCTION


The cardiovascular system is one of the first organs to form and function, and its development is regulated by complex interactions between different cell types as well as several signalling pathways. The angiopoietin/TIE signalling pathway plays major roles in blood and lymphatic vessel development (Iwama et al., 1993; Sato et al., 1993; Dumont et al., 1995; Yano et al., 1997). This signalling is achieved by multiple angiopoietin ligands and two receptor tyrosine kinases, TIE1 (tyrosine-protein kinase receptor 1) (Partanen et al., 1992) and TEK (tyrosine endothelial kinase, also known as TIE2) (Dumont et al., 1993). Both of these receptors are highly enriched in

endothelial cells (ECs) (Armstrong et al., 1993; Batard et al., 1996; Sato et al., 1998), while the ligands are more broadly expressed (Davis et al., 1996; Maisonpierre et al., 1997; Pham et al., 2001). Various missense mutations in *TEK* have been identified in individuals from unrelated families diagnosed with Venous Malformations (OMIM: #600195), one of the most common congenital vascular defects in humans (Calvert et al., 1999; Limaye et al., 2009; Wouters et al., 2010; Amberger et al., 2015). These mutations lead to ligand-independent hyper-phosphorylation of TEK and EC hyperproliferation (Limaye et al., 2009; Soblet et al., 2013; Cai et al., 2019). Upregulation of TEK has also been reported in multiple other diseases, including psoriasis and glioblastoma (Kuroda et al., 2001; Du et al., 2003; Tait and Jones, 2004; Voskas et al., 2005; Souma et al., 2016; Ye et al., 2018). In addition, several heterozygous loss-of-function mutations in *TEK* have been identified in individuals diagnosed with primary congenital glaucoma (Souma et al., 2016). Yet despite the importance of TEK in development and disease, much remains to be investigated about its precise role.

TEK homodimers or heterodimers (with its paralogue TIE1) can directly bind angiopoietins (Davis et al., 1996; Maisonpierre et al., 1997; Valenzuela et al., 1999). The TEK intracellular tyrosine kinase domain becomes auto-phosphorylated upon angiopoietin binding, leading to the activation of multiple downstream pathways that regulate EC proliferation, migration, survival as well as inflammation (Huang et al., 2010; Thurston and Daly, 2012; Eklund et al., 2017). Many *in vivo* studies have shed light on the function of the angiopoietin/TIE signalling pathway. In *TEK* and *TIE1* co-expressing ECs, these two receptors form heterodimers prior to ligand binding. Upon angiopoietin 1 binding, TIE1 is released and TEK/TEK homodimers form (Seegar et al., 2010). However, in *TIE1*-negative ECs, TEK homodimerizes and binds angiopoietins to regulate vascular homeostasis (Saharinen et al., 2005; Seegar et al., 2010). These data suggest that the angiopoietin/TIE signalling pathway is highly context dependent. *Tek* mutant mice die at embryonic day (E) 9.5–10.5 with severe cardiovascular defects, including reduced heart size, disorganized trabeculae, and reduced and hyper-permeable blood vessels (Dumont et al., 1994; Sato et al., 1995). EC-specific *Tek* knockout (KO) mice exhibit similar vascular defects to global *Tek* KO mice, suggesting that TEK functions cell-autonomously during blood vessel development (Chu et al., 2016). Global *Tie1* KO mice die at later stages (E13.5–P0) from haemorrhage (Puri et al., 1995; Sato et al., 1995; D'Amico et al., 2010). Although *Tie1* expression in ECs appears by E7.5–8.75 (Dumont et al., 1995), mutant embryos do not exhibit any obvious vascular defects before E13.5 (Puri et al., 1995; Sato et al., 1995; D'Amico et al., 2010). *Tek;Tie1* double mutant mice exhibit more pronounced vascular defects than the single mutants (Puri et al., 1999; Savant et al., 2015), indicating that these genes have at least some non-overlapping functions during mouse development.

¹Max Planck Institute for Heart and Lung Research, Department of Developmental Genetics, Bad Nauheim 61231, Germany. ²German Centre for Cardiovascular Research (DZHK), Partner Site Rhine-Main, Bad Nauheim 61231, Germany. ³Goethe University Frankfurt am Main, Institute of Cell Biology and Neuroscience, Frankfurt 60438, Germany. ⁴Senckenberg Biodiversity and Climate Research Center (S-BIKF), Frankfurt 60438, Germany. ⁵LOEWE Center for Translational Biodiversity Genomics (TBG), Frankfurt 60438, Germany.

*Authors for correspondence (didier.stainier@mpi-bn.mpg.de, jane.jiang@mpi-bn.mpg.de, ebersberger@em.uni-frankfurt.de)

 Z.J., 0000-0003-3648-8549; C.C., 0000-0003-3716-8539; S.A., 0000-0002-5042-7550; I.E., 0000-0001-8187-9253; D.Y.R.S., 0000-0002-0382-0026

Handling Editor: Steve Wilson

Received 17 May 2020; Accepted 3 September 2020

Zebrafish Tek and Tiel exhibit a high degree of sequence similarity (~70%) with their corresponding murine and human one-to-one orthologues (Lyons et al., 1998; Cunningham et al., 2019). *tek* knockdown (KD) mediated by MO injections has been reported to lead to severe angiogenesis defects, with intersegmental vessel (ISV) ECs displaying reduced proliferation and migration (Li et al., 2014). However, in the ENU-induced *tek*^{hu1667} allele, no obvious vascular phenotypes were observed (Gjini et al., 2011). This premature termination codon (PTC)-bearing mutant is in fact homozygous viable and fertile, even though the mutants display strong nonsense-mediated mRNA decay (NMD) and loss of Tek protein, as detected by immunostaining (Gjini et al., 2011). Thus, while *tek* morphants display severe cardiovascular phenotypes, *tek* mutants do not, leaving unresolved the question of the functional relevance of Tek during zebrafish development.

Phenotypic discrepancies between mutants and morphants in zebrafish have been reported in many studies (Kok et al., 2015; Rossi et al., 2015). These discrepancies could be due to off-target effects of the MOs (Schulte-Merker and Stainier, 2014; Stainier et al., 2015, 2017; Lai et al., 2019), the analysis of hypomorphic alleles (Anderson et al., 2017; Tuladhar et al., 2019; Kim and Zhang, 2020) or transcriptional adaptation (TA), which in some cases can lead to genetic compensation (Rossi et al., 2015; El-Brolosy et al., 2019; Ma et al., 2019). To bypass TA, several strategies have been proposed, including generating small in-frame deletion as well as RNA-less alleles (El-Brolosy and Stainier, 2017; Stainier et al., 2017; El-Brolosy et al., 2019). Similarly, the reliability of MOs has been extensively discussed due to their off-target effects and toxicity (Schulte-Merker and Stainier, 2014; Stainier et al., 2015, 2017; Lai et al., 2019). Deletion of the MO-binding site has been proposed as the only valid control for MO studies (Stainier et al., 2017; Cunningham et al., 2020).

To further investigate the function of Tek in zebrafish development, we generated several loss-of-function *tek* alleles, including RNA-less alleles, an allele lacking the MO-binding site, an in-frame deletion allele and a PTC-containing allele. Our data indicate that none of these mutants exhibits obvious abnormalities during development. Upon MO injections, *tek* mutants lacking the MO-binding site, or the *tek* locus, display arrested angiogenesis around 22 h post fertilization (hpf) and defective ISVs at 48 hpf, as do their MO-injected wild-type siblings, indicating off-target effects of the MO. Thus, although TEK is indispensable for cardiovascular development in mammals, it is not required in zebrafish. In line with these observations, our in-depth evolutionary analyses reveal that the *Tek* gene is absent in all Acanthomorphata (spiny-ray teleosts) species, suggesting a lineage-specific shift in the function of TEK during vertebrate evolution.

RESULTS

Loss-of-function zebrafish *tek* mutants do not exhibit vascular defects

To study the role of TEK during vertebrate development and investigate the phenotypic discrepancy between zebrafish *tek* mutants and morphants, we used the CRISPR/Cas9 genome editing tool (Hwang et al., 2013) to generate several loss-of-function *tek* alleles in zebrafish. These alleles include a PTC allele, *tek*^{bns278}, which contains a 7 bp deletion in exon 15, resulting in a 799 amino acid protein predicted to lack part of the transmembrane domain and the whole tyrosine kinase domain (Fig. 1A). Because small in-frame deletion alleles were previously suggested to be beneficial for gene function studies, as they are unlikely to trigger TA (Stainier et al., 2017; El-Brolosy et al., 2019), we also generated an in-frame deletion allele, *tek*^{bns347} (Fig. 1A; Fig. S1), which affects seven amino acids in

the TK domain and is predicted to be a severe allele (Fig. S1). Furthermore, since RNA-less alleles (i.e. promoter deletions and full-locus deletions) were also reported not to trigger TA (El-Brolosy et al., 2019), we generated two full-locus deletion alleles, *tek*^{bns399} and *tek*^{bns400}, by employing multiple gRNAs targeting the 5' and 3' untranslated regions (UTRs) (Fig. 1A; Fig. S2A,B,D). As an additional control for the MO injection experiments (Stainier et al., 2017), we generated an allele lacking the MO-binding site *tek*^{bns401} (Fig. 1A; Fig. S2A,C,E-G). This allele contains a 261 bp deletion, which includes the 5' UTR and 34 bp of the *tek* coding sequence, and is predicted not to affect protein function (Fig. 1A; Fig. S2A,C,E-G). We first checked *tek* mRNA levels in all generated alleles at 24 hpf by RT-qPCR (Fig. 1B). As expected, the PTC-bearing mutants (*tek*^{bns278}) exhibited a significant decrease in *tek* mRNA levels compared with +/+ siblings, suggesting NMD, whereas the in-frame deletion mutants (*tek*^{bns347}) did not exhibit significantly different mRNA levels compared with +/+ siblings. Furthermore, *tek* expression was not detectable in the full-locus deletion mutants (*tek*^{bns399}, *tek*^{bns400}). The 5' UTR deletion mutants (*tek*^{bns401}) exhibited similar *tek* mRNA levels to +/+ siblings (Fig. 1B). All generated mutants, including their maternal zygotic offspring, are homozygous viable and fertile, as was reported for the ENU-induced *tek*^{hu1667} allele (Gjini et al., 2011). Notably, we did not detect any gross morphological defects in any of the analysed mutants (data not shown). We also performed whole-mount and histological analyses on dissected adult hearts from *tek*^{bns399} full-locus deletion mutants and their +/+ siblings, and found no gross morphological defects, indicating a lack of cardiovascular phenotypes in *tek* mutants during adulthood as well (Fig. S3).

Since *Tek* has been reported to be vital for vascular development in mice (Iwama et al., 1993; Sato et al., 1993; Dumont et al., 1995; Yano et al., 1997), and zebrafish *tek* expression is highly EC enriched (Fig. S4A-C), we focused on blood vessel formation, and yet found no obvious vascular alterations in any of the mutants (Fig. 1C'-H'), when compared with their +/+ siblings (Fig. 1C-H) at 48 hpf. Endothelial *tek* expression in zebrafish embryos can be observed from an early stage, and it appears to be regulated indirectly by Npas4l/Cloche (Marass et al., 2019). Thus, we examined vascular development in detail starting at the 10- to 12-somite stage, when the posterior lateral plate mesoderm migrates to the midline to form the main vessels (Fouquet et al., 1997). We performed this experiment with the in-frame deletion allele and the two RNA-less alleles, and failed to detect any abnormalities (Fig. S5A-D; Fig. S6A-D; Fig. S7A-D). Furthermore, at 24 hpf, ISV length appeared unaffected in all mutants analysed, when compared with their +/+ and +/- siblings (Fig. S5E-H; Fig. S6E-H; Fig. S7E-H). We next hypothesized that these mutants might present subtle phenotypes that would become more prominent when the animals were stressed. Hence, we subjected the embryos to 1 h heat-shock (HS) treatments at 10 and 22 hpf (Marin-Juez et al., 2016). The total ISV length above the yolk extension was then quantified from confocal microscopy images. However, the treated mutant embryos displayed no significant differences when compared with their +/+ and +/- siblings (Fig. S5I-L; Fig. S6I-L). Since *Tek* expression has previously been reported in haematopoietic stem cells (HSCs) in the bone marrow niche (Arai et al., 2004), we also analysed whether loss of *tek* function could lead to blood-related phenotypes. We found that, compared with their +/+ siblings, the full-locus deletion mutants (*tek*^{bns399}) displayed no obvious changes in red blood cell number and wild-type-like mRNA levels of the HSC markers *runx1* and *myb* (previously known as *cmlyb*) at embryonic stages (Fig. S8A-C), as well as normal heart rate (Fig. S8D; Movies 1 and 2) and blood circulation during adulthood (Movies 3 and 4). In summary, we

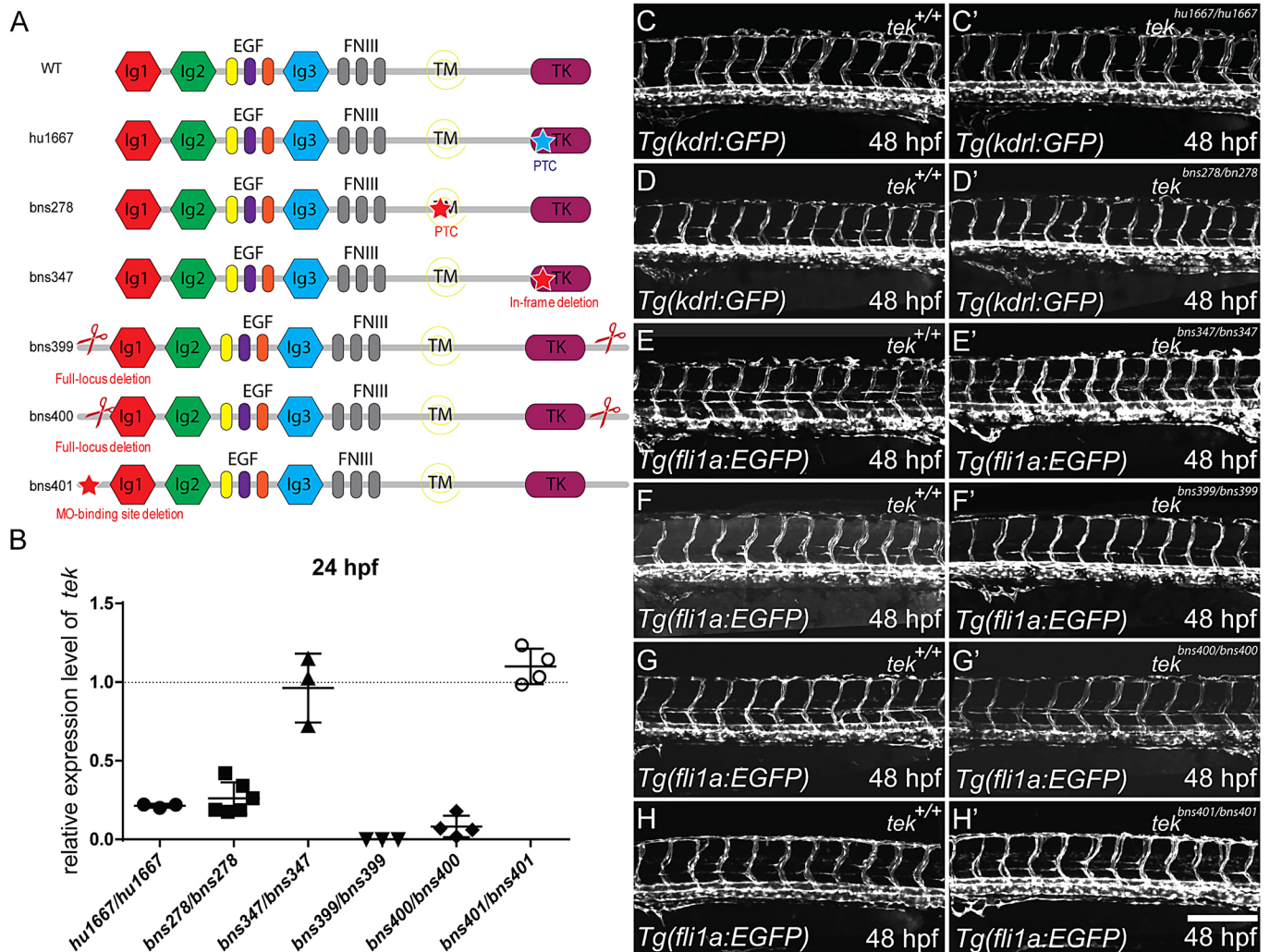


Fig. 1. No gross vascular morphology defects in RNA-less or in-frame deletion zebrafish *tek* mutants. (A) Schematic representation of the Tek protein domains and the lesion in each allele. Blue star represents ENU-induced lesion; red stars and scissors represent CRISPR target sites. Lesions in *tek*^{hu1667} and *tek*^{bns278} result in a premature termination codon in the TK domain- and TM domain-encoding exons, respectively. The lesion in *tek*^{bns347} is an in-frame deletion that is predicted to severely impair Tek function (Fig. S1). *tek*^{bns399} and *tek*^{bns400} are full-locus deletion alleles. *tek*^{bns401} contains a 261 bp deletion around the translational start site. (B) *tek* expression levels in different *tek* mutant alleles when compared with their corresponding +/+ siblings at 24 hpf. (C-H') Lateral views of 48 hpf trunk vessels. No obvious vascular phenotype is observed in any of these alleles (C'-H') when compared with their corresponding +/+ siblings (C-H). PTC, premature termination codon; Ig, immunoglobulin domain; EGF, epidermal growth factor repeat; FNIII, fibronectin type 3 domain; TM, transmembrane domain; TK, tyrosine kinase domain. In B, data are mean±s.d. Scale bar: 200 μm.

generated several loss-of-function *tek* alleles in zebrafish and observed no obvious morphological or cardiovascular phenotypes.

To investigate whether the published *tek*^{hu1667/hu1667} mutants lack a phenotype because of TA-mediated genetic compensation by the *tek* paralogue *tiel* (Gjini et al., 2011), we carried out gene expression analyses. We first performed RT-qPCR at 24 hpf and observed no significant increase in *tiel* mRNA levels in *tek*^{hu1667/hu1667} mutants compared with their +/+ siblings (Fig. S9A). We also examined *tek* and *tiel* expression in 24 hpf *tek*^{hu1667/+} increased embryos by whole-mount *in situ* hybridization (Fig. S9B-E), and observed significantly reduced *tek* expression in *tek*^{hu1667/hu1667} compared with their +/+ siblings (Fig. S9B,C), in line with previous data (Gjini et al., 2011). However, we did not observe obvious changes in *tiel* expression (Fig. S9D,E).

tek morphants display vascular defects

To complement studies with the published translation-blocking MO (ATG1), we also used another non-overlapping MO, *tek*

ATG2 MO, the binding site of which ends 3 bp 5' of the ATG1 MO-binding site (Fig. S2A) (Li et al., 2014). At 48 hpf, control morphants (8 ng) displayed a wild-type-like morphology and a well-established vascular system (Fig. 2A,G). In contrast, *tek* ATG1 morphants (8 ng) exhibited fewer central arteries (CtAs), fewer ECs in the common cardinal veins (CCVs), and defective ISVs (Fig. 2B,E,F,H,K), as previously reported (Li et al., 2014). *tek* ATG2 morphants (8 ng) also exhibited reduced CtA sprouting from the primordial hindbrain channels and fewer ECs in the CCVs. However, we did not observe obvious abnormalities in the large vessels of the trunk in 48 hpf morphants (Fig. 2C,E,F,I,K). We also injected 4 ng of ATG1 MO plus 4 ng of ATG2 MO and observed similar vascular defects in the head and trunk, when compared with 8 ng single MO-injected embryos (Fig. 2D-F,J,K). Taken together, these data corroborate the previous observations that *tek* translation blocking MOs can impair vascular formation (Li et al., 2014).

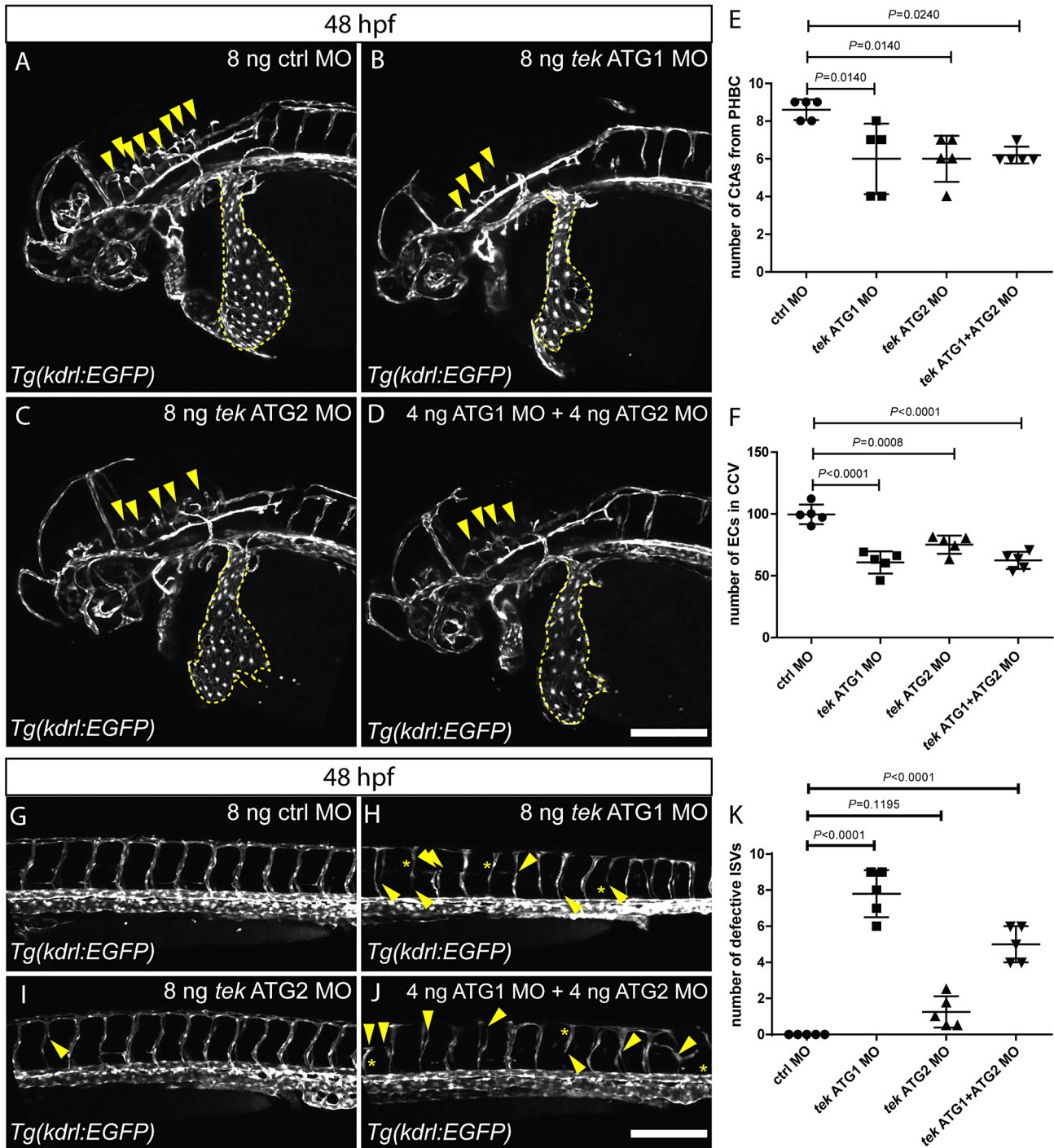


Fig. 2. Zebrafish *tek* morphants display reduced angiogenesis and abnormal CCV formation. (A–D) Lateral views of 48 hpf head vasculature in embryos injected with 8 ng of control MO (A), 8 ng of *tek* ATG1 MO (B), 8 ng of *tek* ATG2 MO (C) or 4 ng of *tek* ATG1 MO plus 4 ng of *tek* ATG2 MO (D). Yellow arrowheads indicate central arteries (CtAs); yellow dashed lines outline the common cardinal veins (CCVs). (E) CtA numbers in different MO-injected groups at 48 hpf. (F) Endothelial cell numbers in the CCVs in different MO-injected groups at 48 hpf. (G–J) Lateral views of 48 hpf trunk vessels in embryos injected with 8 ng of control MO (G), 8 ng of *tek* ATG1 MO (H), 8 ng of *tek* ATG2 MO (I) or 4 ng of *tek* ATG1 MO plus 4 ng of *tek* ATG2 MO (J). Yellow arrowheads indicate abnormal intersegmental vessel (ISV) formation; yellow asterisks indicate absent ISVs. (K) Number of defective ISVs above the yolk extension in different MO-injected groups at 48 hpf. In E, F and K, data are mean \pm s.d. [one-way analysis of variance (ANOVA) followed by Tukey's HSD test]. Scale bars: 200 μ m.

Tek is not required for vascular development in zebrafish

Given the phenotypic differences between *tek* mutants and morphants, and the lack of vascular defects in the full-locus *tek* deletion mutants, we hypothesized that the *tek* morphant phenotypes were due to off-target effects of the MOs. We thus injected various doses of the *tek* ATG1 MO into embryos lacking

the MO-binding site (Fig. 3A), and examined their phenotypes at 22 hpf, 2 h after the initiation of angiogenesis (Isogai et al., 2001). We observed that embryos from *tek^{bns401/+}* crosses exhibited similarly delayed angiogenesis upon *tek* MO injections regardless of their genotype (Fig. 3B,D–I), whereas control morphants displayed no defects (as shown in Fig. 2A,G). These angiogenesis

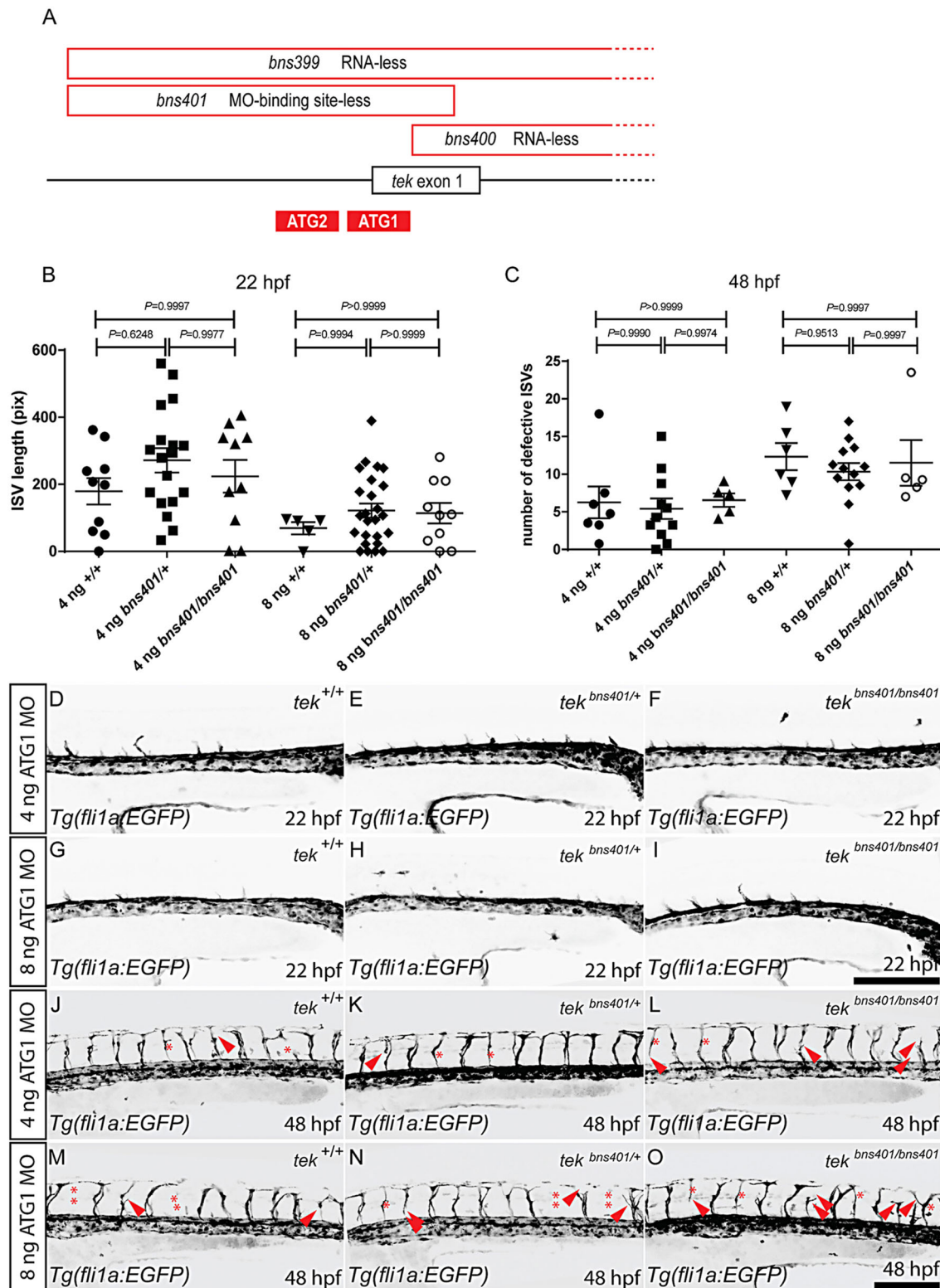


Fig. 3. *tek* MO injections into zebrafish embryos lacking the MO-binding site cause vascular phenotypes. (A) Schematic representation of the deletions in the *tek*^{bns399}, *tek*^{bns400} and *tek*^{bns401} alleles, and the location of the *tek* ATG1 and ATG2 MOs (only the 5' end of the *tek* locus is shown). (B) Total length of 10 intersegmental vessels (ISVs) above the yolk extension in 22 hpf *tek*^{bns401/+} increased embryos injected with 4 or 8 ng of *tek* ATG1 MO. (C) Number of defective ISVs above the yolk extension in 48 hpf *tek*^{bns401/+} increased embryos injected with 4 or 8 ng of *tek* ATG1 MO. (D-F) Lateral views of trunk vessels in 22 hpf *tek*^{bns401/+} increased embryos injected with 4 ng of *tek* ATG1 MO. (G-I) Lateral views of trunk vessels in 22 hpf *tek*^{bns401/+} increased embryos injected with 8 ng of *tek* ATG1 MO. (J-L) Lateral views of trunk vessels in 48 hpf *tek*^{bns401/+} increased embryos injected with 4 ng of *tek* ATG1 MO. (M-O) Lateral views of trunk vessels in 48 hpf *tek*^{bns401/+} increased embryos injected with 8 ng of *tek* ATG1 MO. Red arrowheads indicate abnormal ISV formation; red asterisks indicate absent ISVs. In B and C, data are mean±s.d. [one-way analysis of variance (ANOVA) followed by Tukey's HSD test]. Scale bars: 200 μm.

defects were dose dependent as the embryos injected with 4 ng of *tek* MO displayed a longer total ISV length when compared with the embryos injected with 8 ng of *tek* MO (Fig. 3B). Further examination of the morphant phenotypes at 48 hpf revealed incomplete ISVs, or even absent ISV formation, in all morphants, regardless of their genotype, and again in a dose-dependent manner (Fig. 3C,J-O).

Furthermore, we injected the *tek* ATG1 MO into the *tek*^{bns399} RNA-less allele at several doses (Fig. 4). This allele lacks the entire *tek* coding sequence as well as the ATG1 MO-binding site (Fig. S2A). Again, at 22 hpf, *tek* morphants displayed similar angiogenesis defects regardless of their genotype (Fig. 4A-I), whereas control morphants displayed no defects (as shown in Fig. 2A,G). Similar to what we observed when we injected the MO into mutants lacking the MO-binding site, the morphant phenotypes in *tek*^{bns399/+} incrossed embryos were also dose dependent, as the total ISV length was inversely proportional to the injected dose (Fig. 4I). At 48 hpf, we observed defective ISV formation in all morphants regardless of their genotype (Fig. 4J-R). To assess whether the off-target effects from the *tek* ATG1 MO injections affect *tie1* expression, we analysed *tie1* mRNA and pre-mRNA levels in *tek* morphants. We found that *tie1* mRNA and pre-mRNA levels remained unchanged in *tek* morphants when compared with control (Fig. S9F). In summary, these data indicate that the published vascular defects in *tek* morphants (Li et al., 2014) were due to off-target effects.

The *Tek* gene is absent from a majority of teleost genomes

The angiotensin/TIE signalling pathway plays an essential role in mammalian cardiovascular development (Iwama et al., 1993; Sato et al., 1993; Dumont et al., 1995; Yano et al., 1997). Given that all vertebrates have a cardiovascular system, one might assume that this pathway is similarly essential in bony and cartilaginous fish. Our data, however, show that *Tek* is dispensable in zebrafish. This surprising result suggests a change of *TEK* function during vertebrate evolution. To shed further light on this matter, we investigated the evolutionary history of *Tek* and *Tie1* with a particular focus on the fate of these two genes in ray-finned fish species. Phylogenetic profiling revealed that *Tie1* is consistently present in tetrapods, coelacanth and ray-finned fish, and only individual species are missing a *Tie1* orthologue. *Tie1* is also present in four out of the five analysed ray and shark (Chondrichthyes) genomes (Fig. 5A; Fig. S10; see Files S1 and S2 in the supplementary information). *Tek*, on the other hand, is ubiquitously present in the tetrapods, including coelacanth, and we find orthologues in four out of the five Chondrichthyes. Within the ray-finned fish, however, a huge gap in the phylogenetic profile indicates the absence of the *Tek* gene in most of the analysed fish genomes (Fig. 5A; Fig. S10). Fifty out of the 78 analysed fish species do not have an annotated *Tek* locus, including medaka (*Oryzias latipes*), fugu (*Takifugu rubripes*) and cod (*Gadus morhua*). Reconstruction of the evolutionary history of *Tek* and *Tie1* clarifies the evolutionary scenario (Fig. S5B). *Tek* and *Tie1* can be traced back to a single ancestral gene in the last common ancestor of the vertebrates, as both genes share the same orthologue in sea urchin (*Strongylocentrotus purpuratus*, Echinodermata) and sea squirt (*Ciona intestinalis*, Urochordata). This observation is in line with the previous suggestion that the *SpTie1/2* gene is the sea urchin orthologue of the vertebrate *Tek* and *Tie1* genes (Stevens et al., 2010). Thus, the two paralogous genes, *Tek* and *Tie1*, emerged by a gene duplication in the last common ancestor of the vertebrates, probably as a consequence of the whole-genome duplications that occurred on this lineage (Dehal and Boore, 2005). *Tie1* is present in all analysed

vertebrate species (Fig. 5B; Fig. S10). *Tek* was retained in cartilaginous fish, tetrapods, coelacanth, as well as in early branching ray-finned fish (Fig. 5B; Fig. S10). Interestingly, our analysis reveals a parsimonious explanation for the prominent gap in the phylogenetic profile for *Tek* in ray-finned fish. Loss of a single gene in the last common ancestor of the Acanthomorpha [the largest clade within the teleost family that emerged ~148 million years ago (Chen et al., 2014)] accounts for the absence of *Tek* in a majority of the species analysed (Fig. 5B; Fig. S10). To confirm that the absence of *Tek* in Acanthomorpha is not an artefact caused by incomplete gene annotation, we performed a tBlastN analysis (protein sequence against the translated nucleotide database) (Altschul et al., 1997) in several teleost species with high quality genome assemblies, including medaka, platyfish (*Xiphophorus couchianus*) and stickleback (*Gasterosteus aculeatus*). This analysis revealed no traces of *Tek*. To further increase the resolution of this comparative examination, we investigated the gene neighbourhood around *Tek* across vertebrates (Fig. S11) (Nguyen et al., 2018). This study revealed that whenever *Tek* is present, it is always placed head to tail directly downstream of *Iff74*, or with one intervening gene, and this gene order is conserved from sharks to human (Fig. S11). The shared synteny of *Tek* and *Iff74* indicates that zebrafish and mouse *Tek* are also positional orthologues (Dewey, 2011). Moreover, the conservation of this gene order helps to rule out the unlikely case that all Acanthomorpha genomes suffer from the same genome reconstruction artefact that places *Tek* into an assembly gap. *Iff74* is consistently present throughout the ray-finned fish and also in the Acanthomorpha. We also visually inspected the genomic region around *Iff74* in a subset of Acanthomorpha species, and found no evidence for a consistent assembly artefact across these genomes. In particular, the Fugu assembly is fully closed in this region, showing no traces of *Tek* (Fig. S12). In summary, we conclude that neither a missing gene annotation nor assembly artefacts explain the absence of *Tek* in Acanthomorpha. Instead, there is strong evidence that *Tek* was lost in the Acanthomorpha lineage during evolution, which required that it become functionally dispensable beforehand. To assess whether the angiotensins display a similar evolutionary pattern, we extended the phylogenetic profiles to include angiotensin 1 and angiotensin 2 (Fig. S13; see File S2 in the supplementary information). This analysis, however, revealed no evidence for an accompanying change for these two proteins during evolution.

DISCUSSION

Phenotypic discrepancies between zebrafish *tek* mutants and morphants have been reported (Gjini et al., 2011; Li et al., 2014), leading to questions about the precise function of *tek* during zebrafish development. In this study, we generated and analysed several mutant alleles of *tek*, and integrated these findings with comprehensive evolutionary genetic analyses. Our data indicate that *Tek* is dispensable for zebrafish development.

Systematic examination of gene function

Phenotypic differences between mutants and morphants could result from TA-mediated genetic compensation (Rossi et al., 2015; El-Brolosy et al., 2019; Ma et al., 2019), off-target effects of the MOs (Schulte-Merker and Stainier, 2014; Stainier et al., 2015, 2017; Lai et al., 2019) or the analysis of hypomorphic alleles (Anderson et al., 2017; Tuladhar et al., 2019; Kim and Zhang, 2020). Because of the lack of deficiency alleles in zebrafish and the limited availability of antibodies against zebrafish proteins, it is often hard to determine the relative strength of a mutant allele

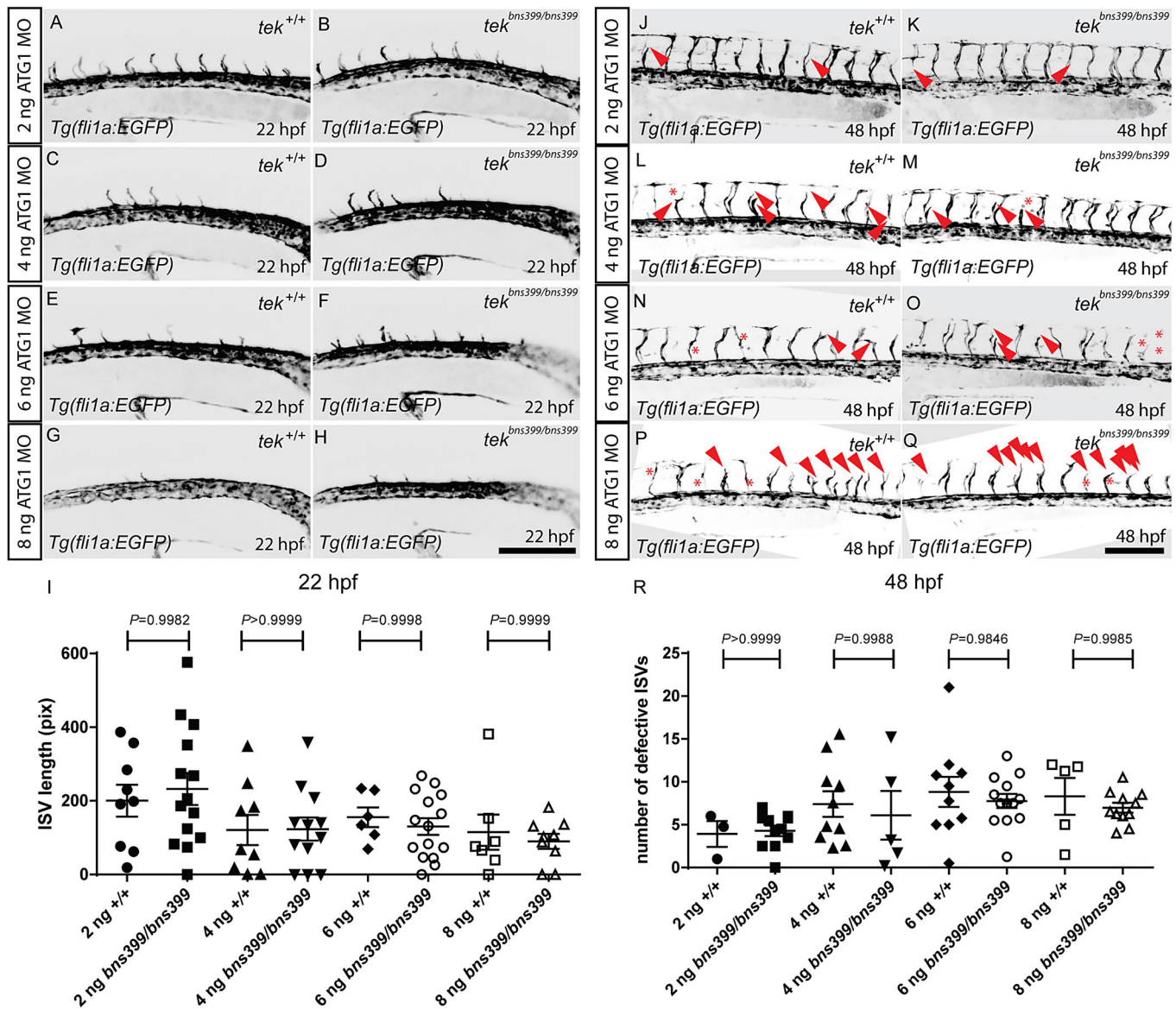


Fig. 4. *tek* MO injections into the zebrafish *tek*^{bns399} RNA-less allele cause vascular phenotypes. (A-H) Lateral views of trunk vessels in 22 hpf *tek*^{bns399/+} increased embryos injected with 2 (A,B), 4 (C,D), 6 (E,F) or 8 (G,H) ng of *tek* ATG1 MO. (I) Total length of 10 intersegmental vessels (ISVs) above the yolk extension in 22 hpf *tek*^{bns399/+} increased embryos injected with 2, 4, 6 or 8 ng of *tek* ATG1 MO. (J-Q) Lateral views of trunk vessels in 48 hpf *tek*^{bns399/+} increased embryos injected with 2 (J,K), 4 (L,M), 6 (N,O) or 8 (P,Q) ng of *tek* ATG1 MO. Red arrowheads indicate abnormal ISV formation; red asterisks indicate absent ISVs. (R) Number of defective ISVs above the yolk extension in 48 hpf *tek*^{bns399/+} increased embryos injected with 2, 4, 6 or 8 ng of *tek* ATG1 MO. In I and R, data are mean±s.d. [by one-way analysis of variance (ANOVA) followed by Tukey's HSD test]. Scale bars: 200 μm.

(Gut et al., 2017). To address these issues, we used multiple gRNAs to target the 5' and 3' UTRs of *tek* and create full-locus deletions. One caveat of this approach is the presence of potential regulatory elements within the deleted area. Therefore, we also generated and analysed other alleles, including a small in-frame deletion allele and a PTC-bearing allele, and observed no obvious phenotypes in any of these mutants (Fig. 1). These data suggest that lack of a phenotype in loss-of-function *tek* mutants is unlikely due to TA-mediated genetic compensation, or to them being hypomorphic alleles. Our genetic experiments provide a systematic examination to determine *Tek* function, and indicate that *Tek* is dispensable for zebrafish development. This conclusion stands in stark contrast to the important roles of mammalian TEK in cardiovascular development, and strongly hints towards a shift of angiopoietin/TIE signalling in function/essentiality during vertebrate evolution.

Possible function of angiopoietin/TIE signalling in zebrafish development

Angiopoietin/TIE signalling is essential for cardiovascular development in mammals; *Tek* and angiopoietin 1 (*Angpt1*)-deficient mouse embryos exhibit severe cardiac defects, as well as abnormal vascular remodelling (Dumont et al., 1994; Sato et al., 1995; Suri et al., 1996; Jeansson et al., 2011). *Tie1* mutant mice exhibit malformed lymphatic sacs and blood vessel remodelling defects (Puri et al., 1995; D'Amico et al., 2010; Qu et al., 2010). Interestingly, no cardiac defects were observed in *Tie1*-deficient mouse embryos (Puri et al., 1995). These data together suggest that murine *Tie1* might be predominantly required for lymphatic vessel formation and remodelling. Previous studies in mouse have also shown that only TEK but not TIE1 has the ability to bind angiopoietins directly (Suri et al., 1996; Maisonpierre et al., 1997). Even though TIE1 was reported to be an orphan receptor,

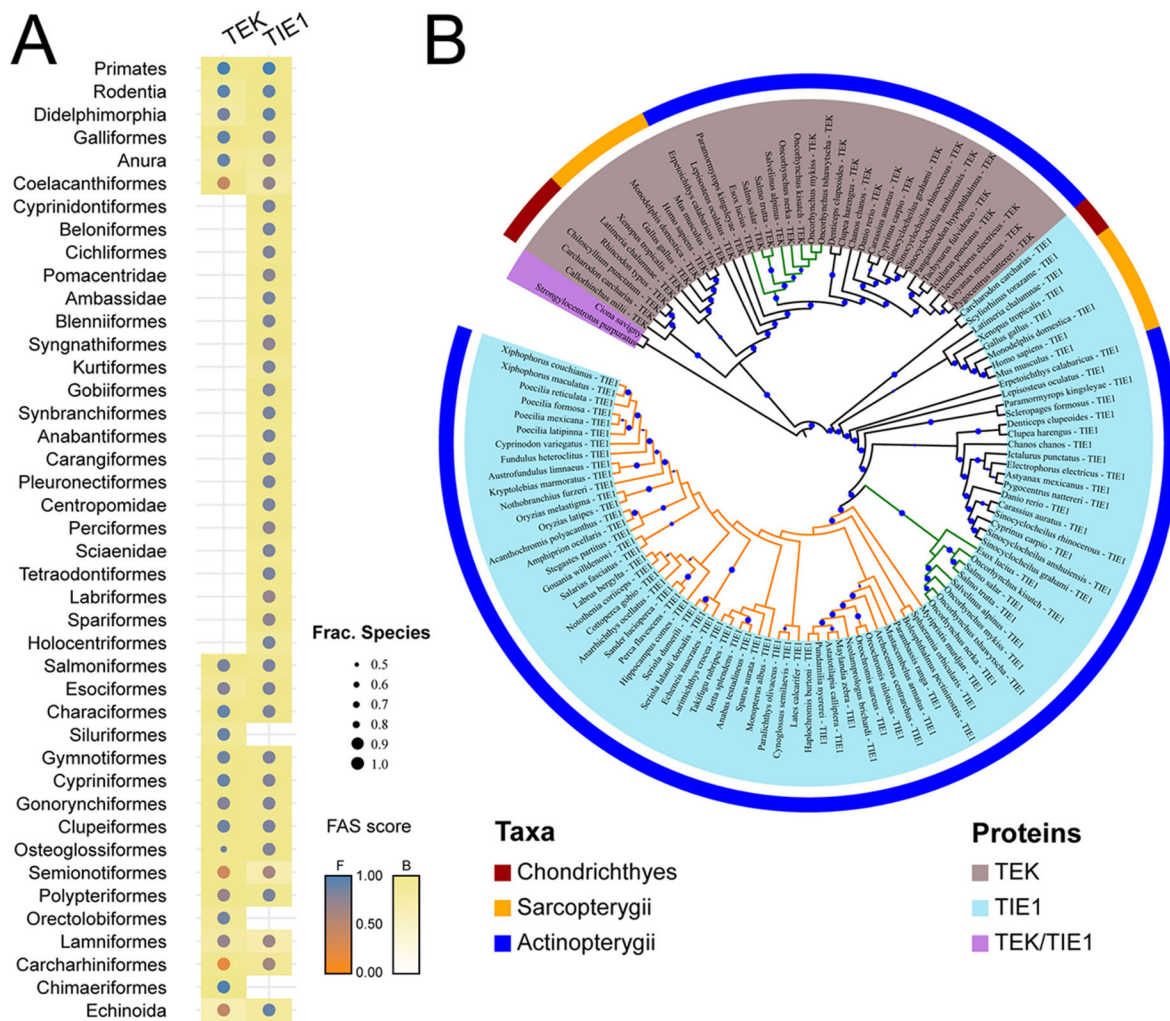


Fig. 5. Loss of *tek* in the Acanthomorpha lineage. (A) Phylogenetic profile of TEK and TIE1 in deuterostomes on the order level. Colour code indicates the feature architecture similarity (FAS) score of the orthologues to the human seed protein. Dot size indicates the fraction of species subsumed in an order that carries an orthologue to the respective protein. (B) Phylogeny of TEK and TIE1. The coloured ring segments represent the three main vertebrate groups. TEK/TIE1 represents the primordial protein outside the vertebrates; TEK and TIE1 are each indicated by coloured taxa. The Acanthomorpha and their sister clade, the Salmoniformes, are indicated by orange and green branches, respectively. Branch labels reflect the percent bootstrap support, where the dot size is proportional to the support value. Only branches with a minimum bootstrap support of 50 are labelled. The tree is provided in Newick format in File S1 in the supplementary information, and the protein IDs of the TEK and TIE1 orthologues together with the protein sequences are provided in File S2 in the supplementary information.

angiopoietin 1 can stimulate TIE1 phosphorylation, and this activation is enhanced by the presence of TEK (i.e. a TIE1/TEK heterodimer) (Marron et al., 2000; Saharinen et al., 2005). While angiopoietin 1 is an agonist of TEK, angiopoietin 2 is a context-dependent agonist/antagonist of TEK (Davis et al., 1996; Maisonpierre et al., 1997). All major angiopoietins are present in the zebrafish genome (Pham et al., 2001). As in mammals, *angpt1* and *angpt2* in zebrafish have been reported to be required for cardiovascular development, based on MO experiments (Lamont et al., 2010; Li et al., 2014). We found that loss-of-function *tek* mutants in zebrafish display no obvious morphological or cardiovascular defects, whereas mammalian *Tek* mutants display severe cardiovascular defects (Dumont et al., 1994; Sato et al., 1995). On the other hand, *tie1* mutants in zebrafish display severe cardiovascular defects (Carlantoni et al., 2020). Thus, it is possible that in zebrafish TIE1 has fully or partially overtaken the function of Tek. Similarly, in other fish species that have lost the *tek* locus, TIE1 might be solely responsible for angiopoietin/TIE signalling.

Evolutionary analyses facilitate gene function studies

The emergence of novel gene functions is often preceded by the duplication of an ancestral gene followed by the functional diversification of the paralogues (Ohno, 1970; Magadum et al., 2013). Our data suggest that *Tek* and *Tie1* emerged by a gene duplication event in the last common ancestor of the vertebrates (Fig. 5B). Experimental evidence in human and mouse has revealed that both genes are actively involved in angiopoietin/TIE signalling in mammalian cardiovascular development. The maintenance of the two paralogues over more than 450 million years (dos Reis et al., 2015) indicates that they have assumed distinct and essential roles during their evolution. Given that all vertebrates have a cardiovascular system, it seems natural to hypothesize that the involvement of Tek and TIE1 in vascular formation represents the ancestral state, and that both proteins are similarly essential in zebrafish. However, our results are at odds with this scenario. Although both *tek* and *tie1* are present in the zebrafish genome, Tek is functionally dispensable for zebrafish development. Moreover, our phylogenetic profiling reveals that this

gene is entirely absent in the Acanthomorpha lineage, which comprises about 60% of the contemporary teleost species, and about one-third of all vertebrate species (Alfaro et al., 2018). This observation strongly indicates that angiotensin/TIE signalling is evolutionarily more plastic than hitherto assumed. Although both *Tek* and *Tie1* were present in the last common ancestor of mammals and ray-finned fish, our results show that their precise roles in cardiovascular development remain to be determined. It is still tempting to speculate that TEK and TIE1 have been as important as they are in contemporary mammals, and that TEK lost its essentiality in the teleost lineage. However, it appears similarly parsimonious to hypothesize that TEK gained its essential role only after the ray-finned fish split from the tetrapod lineage. Surprisingly, preliminary evidence may in fact hint towards the latter hypothesis. Increasing the resolution of the phylogenetic profiles to the level of protein feature architecture reveals that both mammalian TEK and TIE1 have experienced a lineage specific modification in their architecture: Mammalian TEK displays a unique ligand-binding Ig2 domain architecture; TIE1, in turn, has gained a proline/glycine-rich domain at its N-terminus (Fig. S14A,B). It will be interesting to determine whether this proline-rich domain is involved in protein-protein interactions and signalling complex assembly (Kay et al., 2000). Functional studies on the protein domain level complemented with studies examining the essentiality of TEK and TIE1 in both early branching tetrapods (e.g. western clawed frog, *Xenopus tropicalis*) and early branching ray-finned fish (e.g. spotted gar, *Lepisosteus oculatus*) will help to clarify on which evolutionary lineage and in which direction the potential functional transition of TEK occurred.

MATERIALS AND METHODS

Zebrafish husbandry and strains

All zebrafish (*Danio rerio*) were maintained under standard conditions according to institutional (Max Planck Society) and national ethical and animal welfare guidelines approved by the ethics committee for animal experiments at the Regierungspräsidium Darmstadt, Germany (permit number B2/1218) as well as the FELASA guidelines (Alestrom et al., 2019). The following zebrafish lines were used: *Tg(fli1a:EGFP)^{y1}* (Lawson and Weinstein, 2002) and *Tg(kdr1:EGFP)^{s843}* (Jin et al., 2005).

Genome editing by CRISPR/Cas9

CRISPR gRNA design was performed using online tools https://eu.idtdna.com/site/order/designtool/index/CRISPR_SEQUENCE and <http://chopchop.cbu.uib.no/>. gRNAs were generated with gRNA specific primers (Thermo Fisher Scientific) as previously described (Hwang et al., 2013). gRNAs were transcribed with the MEGAshortscript T7 Transcription Kit (Thermo Fisher Scientific) followed by purification with the RNA Clean and Concentrator kit (Zymo Research). The PTC-containing allele *tek^{bns278}* and the in-frame deletion allele *tek^{bns347}* were generated with single gRNA targeting the corresponding tyrosine kinase domain. The RNA-less *tek^{bns399}* and *tek^{bns400}* alleles and the 5'UTR deletion *tek^{bns401}* allele were generated with different sets of gRNAs as illustrated in Fig. 1. Notably, the *tek^{bns401}* mutation is predicted not to impair Tek function, due to a downstream ATG present in the 1st exon. All gRNAs used for CRISPR/Cas9 genome editing are listed in Table S1.

Whole-mount *in situ* hybridization and O-Dianisidine staining

tek and *tie1* *in situ* probes were generated by PCR amplification from 24 hpf zebrafish cDNA using the primer sets listed in Table S1. PCR products were subsequently transcribed with T7 or SP6 RNA polymerases (Promega) followed by purification using an RNA Clean and Concentrator kit (Zymo Research). Whole-mount colorimetric *in situ* hybridization was performed as previously described (Thambyrajah et al., 2016). Embryos were obtained from heterozygous incrosses and they were processed together throughout the *in situ* protocol followed by genotyping. O-Dianisidine staining was performed on 48 hpf dechorionated embryos for 15 min in the dark at room temperature with staining solution (600 µg/ml O-Dianisidine, 6.5% H₂O₂,

40% ethanol and 0.1 M sodium acetate) followed by 15 min room temperature fixation in 4% PFA and five PBS washes (5 min each). Embryos for O-Dianisidine staining were obtained from *tek^{bns399/bns399}* incrosses and wild-type sibling incrosses.

Histological analysis of adult zebrafish heart

Histological analyses were performed as previously described (Marin-Juez et al., 2016). Primary antibodies used include anti-myosin heavy chain (MF20; DSHB) at 1:100 and anti-GFP (Aves Labs, GFP-1010) at 1:200. Secondary antibodies used include Alexa goat anti-chicken 488 (Invitrogen, A-11039) at 1:500 and Alexa donkey anti-mouse 568 (Invitrogen, A10037) at 1:500. The third mutant heart (full-locus deletion) displayed reduced coronary vessel coverage without gross morphological defects, which could be due to delayed development during husbandry.

Injections

MOs were injected directly into the yolk of one-cell stage embryos. All MO sequences are listed in Table S1. gRNA(s) and *Cas9* mRNA were injected together into the cell of one-cell stage embryos (100 pg *Cas9* mRNA and 100 pg gRNAs). Capped *Cas9* mRNA was synthesized using the mMACHINE T3 Transcription kit (Thermo Fisher Scientific) and purified using an RNA Clean and Concentrator kit (Zymo Research).

cDNA synthesis and RT-qPCR

Total RNA was extracted using 100 µl TRIzol Reagent (Thermo Fisher Scientific). At least 500 ng of RNA was used for reverse transcription using the Maxima First Strand cDNA synthesis kit (Thermo Fisher Scientific). RT-qPCR was performed in a CFX Connect Real-Time System (Bio-Rad). All reactions were performed in technical triplicates from at least three biological replicates using the SYBR Green PCR Master Mix (Thermo Fisher Scientific). Results were normalized to *rpl13a* expression. Ct values for the reference gene ranged between 12 and 21. All primers used for the RT-qPCR experiments are listed in Table S1. All Ct values are listed in Table S2.

Genotyping

Genomic DNA was extracted using 10-50 µl 50 mM NaOH as previously described (Wilkinson et al., 2013) or recovered from the lower organic layer following single embryo RNA extraction with 100 µl TRIzol Reagent (Thermo Fisher Scientific). *tek^{hul1667}*, *tek^{bns278}* and *tek^{bns347}* animals were genotyped with high-resolution melt (HRM) analysis (Samarut et al., 2016). Standard PCR was used to genotype the *tek^{bns399}* and *tek^{bns400}* RNA-less alleles and the 5'UTR deletion allele *tek^{bns401}*. All primers used for genotyping are listed in Table S1.

Heat-shock treatments

Embryos were raised at 28.5°C and then subjected to a 39°C heat-shock for 1 h by replacing the egg water with pre-warmed (39°C) egg water at 10 and 22 hpf, and kept in a 39°C incubator as previously described (Marin-Juez et al., 2016).

Confocal microscopy and image processing

Fluorescent images of zebrafish embryos were acquired using a Zeiss LSM 700 confocal microscope (Plan-Apochromat 10×/0.45 objective lens) or a Zeiss Lightsheet Z.1. microscope (5× objective lens). Adult heart section images were acquired with an inverted Zeiss Cell Observer SD microscope, equipped with a Yokogawa CSU-X1 spinning disk (20× objective lens). Embryos were mounted in 1% UltraPure Low Melting Point Agarose (Thermo Fisher Scientific) in egg water with tricaine in a glass-bottomed Petri dish (MatTek) or a capillary tube (Zeiss). Images and videos of whole-mount embryos and whole hearts were obtained using a Nikon SMZ25 stereomicroscope. Obtained images were subsequently processed with ZEN (black edition), and image analysis was performed using ImageJ. All figures were prepared using Adobe Photoshop 2020 and Adobe Illustrator 2020.

PROVEAN prediction

Protein function prediction was performed with the Protein Variation Effect Analyser (PROVEAN) (<http://provean.jcvi.org/index.php>) as previously described (Choi and Chan, 2015).

Gene order analyses

Gene order analyses were performed with Genomicus version 99.01 (<https://www.genomicus.biologie.ens.fr/genomicus-99.01/cgi-bin/search.pl>) under custom view with the Chordata root species, as previously described (Nguyen et al., 2018).

Evolutionary analysis of TEK, TIE1 and angiopoietins

We used HaMStR-OneSeq v1.8.0 (Ebersberger et al., 2014) (<https://github.com/BIONF/HaMStR>) to determine the presence-absence pattern of orthologues to human TEK (UniprotID: Q02763), TIE1 (UniprotID: P35590), angiopoietin 1 (UniprotID: Q15389) and angiopoietin 2 (UniprotID: O15123) across 255 species represented in the RefSeq partition of non-mammalian vertebrate genomes available at NCBI Genome (February 2020) (<https://ftp.ncbi.nlm.nih.gov/genomes/refseq/>), complemented with the Quest For Orthologs reference proteomes (https://www.ebi.ac.uk/reference_proteomes/), and with the sea urchin (*Strongylocentrotus purpuratus*) proteome from NCBI Genome. The full list of taxa is provided in Table S3. Pairwise protein feature architecture similarities (Koestler et al., 2010) between the human seed proteins and their respective orthologues were assessed and scored with feature architecture similarity (<https://github.com/BIONF/FAS>). Phylogenetic profiles together with the protein feature architecture were visualized and analysed with PhyloProfile (Tran et al., 2018). Representative orthologues from five sarcopterygians, 76 actinopterygians and five chondrichthyans, and from two chordate outgroup species were aligned with Muscle v3.8.31 (Edgar, 2004), and alignment columns with more than 50% gaps were excluded prior to phylogeny reconstruction using a custom Perl script. The processed alignment served as an input for a maximum likelihood tree reconstruction with RAxML v.8.2.11 (Stamatakis, 2014) choosing the option to automatically select the optimal model of sequence evolution (option PROTGAMMAAUTO). Branch support was assessed with 100 non-parametric bootstrap replicates using the rapid bootstrapping algorithm implemented into RAxML (Stamatakis et al., 2008). Tree display and editing were performed with iTOL (Letunic and Bork, 2019).

Statistics

Statistical analysis was performed using GraphPad Prism 6. *P*-values were determined using the Mann–Whitney *U* test for comparison of two samples, one-way analysis of variance (ANOVA) followed by Tukey's HSD test for comparison of at least three samples or two-way analysis of variance (ANOVA) followed by Tukey's HSD test for comparison of at least three grouped samples. Data are mean±s.d.

Acknowledgement

We thank Rubén Marín Juez, Felix Gunawan, Samuel Capon, Kenny Mattonet, Sebastien Gauvrit, Vahan Seroby and Mohamed El-Brolosy for discussions and/or comments on the manuscript, and Ngoc Vinh Tran for support in the phylogenetic profiling analysis.

Competing interests

The authors declare no competing or financial interests.

Author contributions

Conceptualization: Z.J., D.Y.R.S.; Methodology: Z.J., C.C., S.A., I.E.; Validation: Z.J.; Formal analysis: Z.J., I.E.; Investigation: Z.J.; Resources: D.Y.R.S.; Data curation: Z.J.; Writing - original draft: Z.J., I.E., D.Y.R.S.; Writing - review & editing: Z.J., C.C., S.A., I.E., D.Y.R.S.; Visualization: Z.J., I.E.; Supervision: D.Y.R.S.; Project administration: D.Y.R.S.; Funding acquisition: I.E., D.Y.R.S.

Funding

This research was supported by funds from the Max-Planck-Gesellschaft, the European Research Council (ERC-2015-AdG - 694455), the Deutsche Forschungsgemeinschaft and the Fondation Leducq (15 CVD 03 to D.Y.R.S.), and by the research funding program Landes-Offensive zur Entwicklung Wissenschaftlich-ökonomischer Exzellenz (LOEWE) of the State of Hessen, Research Center for Translational Biodiversity Genomics (TBG) to I.E.

Data availability

Phylogenetic data are available from the Dryad Digital Repository (Jiang et al., 2020): [dryad.np5hqbzr0](https://doi.org/10.2202/dryad.np5hqbzr0)

Supplementary information

Supplementary information available online at <https://dev.biologists.org/lookup/doi/10.1242/dev.193029.supplemental>

References

- Alestrom, P., D'Angelo, L., Midtlyng, P. J., Schorderet, D. F., Schulte-Merker, S., Sohm, F. and Warner, S. (2019). Zebrafish: housing and husbandry recommendations. *Lab Anim-UK* **54**, 213–224. doi:10.1177/0023677219869037
- Alfaro, M. E., Faircloth, B. C., Harrington, R. C., Sorenson, L., Friedman, M., Thacker, C. E., Oliveros, C. H., Černý, D. and Near, T. J. (2018). Explosive diversification of marine fishes at the Cretaceous-Palaeogene boundary. *Nat. Ecol. Evol.* **2**, 688–696. doi:10.1038/s41559-018-0494-6
- Altschul, S. F., Madden, T. L., Schaffer, A. A., Zhang, J., Zhang, Z., Miller, W. and Lipman, D. J. (1997). Gapped BLAST and PSI-BLAST: a new generation of protein database search programs. *Nucleic Acids Res.* **25**, 3389–3402. doi:10.1093/nar/25.17.3389
- Amberger, J. S., Bocchini, C. A., Schiettecatte, F., Scott, A. F. and Hamosh, A. (2015). OMIM.org: online mendelian inheritance in man (OMIM(R)), an online catalog of human genes and genetic disorders. *Nucleic Acids Res.* **43**, D789–D798. doi:10.1093/nar/gku1205
- Anderson, J. L., Mulligan, T. S., Shen, M.-C., Wang, H., Scahill, C. M., Tan, F. J., Du, S. J., Busch-Nentwich, E. M. and Farber, S. A. (2017). mRNA processing in mutant zebrafish lines generated by chemical and CRISPR-mediated mutagenesis produces unexpected transcripts that escape nonsense-mediated decay. *PLoS Genet.* **13**, e1007105. doi:10.1371/journal.pgen.1007105
- Arai, F., Hirao, A., Ohmura, M., Sato, H., Matsuoka, S., Takubo, K., Ito, K., Koh, G. Y. and Suda, T. (2004). Tie2/angiopoietin-1 signaling regulates hematopoietic stem cell quiescence in the bone marrow niche. *Cell* **118**, 149–161. doi:10.1016/j.cell.2004.07.004
- Armstrong, E., Korhonen, J., Silvennoinen, O., Cleveland, J. L., Lieberman, M. A. and Alitalo, R. (1993). Expression of tie receptor tyrosine kinase in leukemia cell lines. *Leukemia* **7**, 1585–1591.
- Batard, P., Sansilvestri, P., Scheinecker, C., Knapp, W., Debili, N., Vainchenker, W., Buhring, H. J., Monier, M. N., Kukk, E., Partanen, J. et al. (1996). The Tie receptor tyrosine kinase is expressed by human hematopoietic progenitor cells and by a subset of megakaryocytic cells. *Blood* **87**, 2212–2220. doi:10.1182/blood.V87.6.2212.bloodjournal8762212
- Cai, Y., Schrenk, S., Goines, J., Davis, G. E. and Boscolo, E. (2019). Constitutive active mutant *TIE2* induces enlarged vascular lumen formation with loss of apical polarity and pericyte recruitment. *Sci. Rep.* **9**, 12352. doi:10.1038/s41598-019-48854-2
- Calvert, J. T., Riney, T. J., Kontos, C. D., Cha, E. H., Prieto, V. G., Shea, C. R., Berg, J. N., Nevin, N. C., Simpson, S. A., Pasyk, K. A. et al. (1999). Allelic and locus heterogeneity in inherited venous malformations. *Hum. Mol. Genet.* **8**, 1279–1289. doi:10.1093/hmg/8.7.1279
- Carlantoni, C., Allanki, S., Kontarakis, Z., Rossi, A., Piesker, J., Günther, S. and Stainier, D. Y. R. (2020). Tie1 regulates zebrafish cardiac morphogenesis through tollid-like 1 expression. *Dev. Biol.* (in press). doi:10.1016/j.ydbio.2020.09.008
- Chen, W.-J., Santini, F., Carnevale, G., Chen, J.-N., Liu, S.-H., Lavoué, S. and Mayden, R. L. (2014). New insights on early evolution of spiny-rayed fishes (Teleostei: Acanthomorpha). *Front. Mar. Sci.* **1**, 53. doi:10.3389/fmars.2014.00053
- Choi, Y. and Chan, A. P. (2015). PROVEAN web server: a tool to predict the functional effect of amino acid substitutions and indels. *Bioinformatics* **31**, 2745–2747. doi:10.1093/bioinformatics/btv195
- Chu, M., Li, T., Shen, B., Cao, X., Zhong, H., Zhang, L., Zhou, F., Ma, W., Jiang, H., Xie, P. et al. (2016). Angiopoietin receptor Tie2 is required for vein specification and maintenance via regulating COUP-TFII. *eLife* **5**, e21032. doi:10.7554/eLife.21032.018
- Cunningham, F., Achuthan, P., Akanni, W., Allen, J., Amode, M. R., Armean, I. M., Bennett, R., Bhari, J., Billis, K., Boddou, S. et al. (2019). Ensembl 2019. *Nucleic Acids Res.* **47**, D745–D751. doi:10.1093/nar/gky1113
- Cunningham, C. M., Bellipanni, G., Habas, R. and Balciunas, D. (2020). Deletion of morpholino binding sites (DeMOBS) to assess specificity of morphant phenotypes. *Sci. Rep.* **10**, 15366. doi:10.1038/s41598-020-71708-1
- D'Amico, G., Korhonen, E. A., Waltari, M., Saharinen, P., Laakkonen, P. and Alitalo, K. (2010). Loss of endothelial Tie1 receptor impairs lymphatic vessel development—brief report. *Arterioscler. Thromb. Vasc. Biol.* **30**, 207–209. doi:10.1161/ATVBAHA.109.196618
- Davis, S., Aldrich, T. H., Jones, P. F., Acheson, A., Compton, D. L., Jain, V., Ryan, T. E., Bruno, J., Radziejewski, C., Maisonpierre, P. C. et al. (1996). Isolation of angiopoietin-1, a ligand for the TIE2 receptor, by secretion-trap expression cloning. *Cell* **87**, 1161–1169. doi:10.1016/S0092-8674(00)81812-7
- Dehal, P. and Boore, J. L. (2005). Two rounds of whole genome duplication in the ancestral vertebrate. *PLoS Biol.* **3**, e314. doi:10.1371/journal.pbio.0030314
- Dewey, C. N. (2011). Positional orthology: putting genomic evolutionary relationships into context. *Brief. Bioinform.* **12**, 401–412. doi:10.1093/bib/bbr040
- dos Reis, M., Thawornwattana, Y., Angelis, K., Telford, M. J., Donoghue, P. C. and Yang, Z. (2015). Uncertainty in the timing of origin of animals and the limits of

- precision in molecular timescales. *Curr. Biol.* **25**, 2939-2950. doi:10.1016/j.cub.2015.09.066
- Du, L., Sullivan, C. C., Chu, D., Cho, A. J., Kido, M., Wolf, P. L., Yuan, J. X.-J., Deutsch, R., Jamieson, S. W. and Thistlethwaite, P. A. (2003). Signaling molecules in nonfamilial pulmonary hypertension. *N. Engl. J. Med.* **348**, 500-509. doi:10.1056/NEJMoa021650
- Dumont, D. J., Gradwohl, G. J., Fong, G. H., Auerbach, R. and Breitman, M. L. (1993). The endothelial-specific receptor tyrosine kinase, Tek, is a member of a new subfamily of receptors. *Oncogene* **8**, 1293-1301.
- Dumont, D. J., Gradwohl, G., Fong, G. H., Puri, M. C., Gertsenstein, M., Auerbach, A. and Breitman, M. L. (1994). Dominant-negative and targeted null mutations in the endothelial receptor tyrosine kinase, tek, reveal a critical role in vasculogenesis of the embryo. *Genes Dev.* **8**, 1897-1909. doi:10.1101/gad.8.16.1897
- Dumont, D. J., Fong, G. H., Puri, M. C., Gradwohl, G., Alitalo, K. and Breitman, M. L. (1995). Vascularization of the mouse embryo: a study of *flk-1*, *tek*, *tie*, and vascular endothelial growth factor expression during development. *Dev. Dyn.* **203**, 80-92. doi:10.1002/aja.1002030109
- Ebersberger, I., Simm, S., Leisegang, M. S., Schmitzberger, P., Mirus, O., von Haeseler, A., Bohnsack, M. T. and Schleiff, E. (2014). The evolution of the ribosome biogenesis pathway from a yeast perspective. *Nucleic Acids Res.* **42**, 1509-1523. doi:10.1093/nar/gkt1137
- Edgar, R. C. (2004). MUSCLE: multiple sequence alignment with high accuracy and high throughput. *Nucleic Acids Res.* **32**, 1792-1797. doi:10.1093/nar/gkh340
- Eklund, L., Kangas, J. and Saharinen, P. (2017). Angiotensin-Tie signalling in the cardiovascular and lymphatic systems. *Clin. Sci. (Lond.)* **131**, 87-103. doi:10.1042/CS20160129
- El-Brolosy, M. A. and Stainier, D. Y. R. (2017). Genetic compensation: a phenomenon in search of mechanisms. *PLoS Genet.* **13**, e1006780. doi:10.1371/journal.pgen.1006780
- El-Brolosy, M. A., Kontarakis, Z., Rossi, A., Kuenne, C., Gunther, S., Fukuda, N., Kikhi, K., Boezio, G. L. M., Takacs, C. M., Lai, S. L. et al. (2019). Genetic compensation triggered by mutant mRNA degradation. *Nature* **568**, 193-197. doi:10.1038/s41586-019-1064-z
- Fouquet, B., Weinstein, B. M., Serluca, F. C. and Fishman, M. C. (1997). Vessel patterning in the embryo of the zebrafish: guidance by notochord. *Dev. Biol.* **183**, 37-48. doi:10.1006/dbio.1996.8495
- Gjini, E., Hekking, L. H., Kuchler, A., Saharinen, P., Wienholds, E., Post, J. A., Alitalo, K. and Schulte-Merker, S. (2011). Zebrafish Tie-2 shares a redundant role with Tie-1 in heart development and regulates vessel integrity. *Dis. Model. Mech.* **4**, 57-66. doi:10.1242/dmm.005033
- Gut, P., Reischauer, S., Stainier, D. Y. R. and Arnaout, R. (2017). Little fish, big data: zebrafish as a model for cardiovascular and metabolic disease. *Physiol. Rev.* **97**, 889-938. doi:10.1152/physrev.00038.2016
- Huang, H., Bhat, A., Woodnutt, G. and Lappe, R. (2010). Targeting the ANGPT-TIE2 pathway in malignancy. *Nat. Rev. Cancer* **10**, 575-585. doi:10.1038/nrc2894
- Hwang, W. Y., Fu, Y., Reyon, D., Maeder, M. L., Tsai, S. Q., Sander, J. D., Peterson, R. T., Yeh, J. R. and Jung, J. K. (2013). Efficient genome editing in zebrafish using a CRISPR-Cas system. *Nat. Biotechnol.* **31**, 227-229. doi:10.1038/nbt.2501
- Isogai, S., Horiguchi, M. and Weinstein, B. M. (2001). The vascular anatomy of the developing zebrafish: an atlas of embryonic and early larval development. *Dev. Biol.* **230**, 278-301. doi:10.1006/dbio.2000.9995
- Iwama, A., Hamaguchi, I., Hashiyama, M., Murayama, Y., Yasunaga, K. and Suda, T. (1993). Molecular cloning and characterization of mouse TIE and TEK receptor tyrosine kinase genes and their expression in hematopoietic stem cells. *Biochem. Biophys. Res. Commun.* **195**, 301-309. doi:10.1006/bbrc.1993.2045
- Jeansson, M., Gawlik, A., Anderson, G., Li, C., Kerjaschki, D., Henkelman, M. and Quaggin, S. (2011). Angiotensin-1 is essential in mouse vasculature during development and in response to injury. *J. Clin. Invest.* **121**, 2278-2289. doi:10.1172/JCI46322
- Jiang, Z., Carlantoni, C., Allanki, S., Ebersberger, I. and Stainier, D. Y. R. (2020). Data from: Tek/Tie2 is not required for cardiovascular development in zebrafish. *Dryad Digital Repository* doi: 10.5061/dryad.np5hqbzr0
- Jin, S. W., Beis, D., Mitchell, T., Chen, J. N. and Stainier, D. Y. (2005). Cellular and molecular analyses of vascular tube and lumen formation in zebrafish. *Development* **132**, 5199-5209. doi:10.1242/dev.02087
- Kay, B. K., Williamson, M. P. and Sudol, M. (2000). The importance of being proline: the interaction of proline-rich motifs in signaling proteins with their cognate domains. *FASEB J.* **14**, 231-241. doi:10.1096/fasebj.14.2.231
- Kim, B. H. and Zhang, G. (2020). Generating stable knockout zebrafish lines by deleting large chromosomal fragments using Multiple gRNAs. *G3 (Bethesda)* **10**, 1029-1037. doi:10.1534/g3.119.401035
- Koestler, T., von Haeseler, A. and Ebersberger, I. (2010). FACT: functional annotation transfer between proteins with similar feature architectures. *BMC Bioinformatics* **11**, 417. doi:10.1186/1471-2105-11-417
- Kok, F. O., Shin, M., Ni, C. W., Gupta, A., Grosse, A. S., van Impel, A., Kirchmaier, B. C., Peterson-Maduro, J., Kourkoulis, G., Male, I. et al. (2015). Reverse genetic screening reveals poor correlation between morpholino-induced and mutant phenotypes in zebrafish. *Dev. Cell* **32**, 97-108. doi:10.1016/j.devcel.2014.11.018
- Kuroda, K., Sapadin, A., Shoji, T., Fleischmajer, R. and Lebwohl, M. (2001). Altered expression of angiotensins and Tie2 endothelium receptor in psoriasis. *J. Invest. Dermatol.* **116**, 713-720. doi:10.1046/j.1523-1747.2001.01316.x
- Lai, J. K. H., Gagalova, K. K., Kuenne, C., El-Brolosy, M. A. and Stainier, D. Y. R. (2019). Induction of interferon-stimulated genes and cellular stress pathways by morpholinos in zebrafish. *Dev. Biol.* **454**, 21-28. doi:10.1016/j.ydbio.2019.06.008
- Lamont, R. E., Vu, W., Carter, A. D., Serluca, F. C., MacRae, C. A. and Childs, S. J. (2010). Hedgehog signaling via angiotensin1 is required for developmental vascular stability. *Mech. Dev.* **127**, 159-168. doi:10.1016/j.mod.2010.02.001
- Lawson, N. D. and Weinstein, B. M. (2002). In vivo imaging of embryonic vascular development using transgenic zebrafish. *Dev. Biol.* **248**, 307-318. doi:10.1006/dbio.2002.0711
- Letunic, I. and Bork, P. (2019). Interactive tree of life (iTOL) v4: recent updates and new developments. *Nucleic Acids Res.* **47**, W256-W259. doi:10.1093/nar/gkz239
- Li, W., Chen, J., Deng, M. and Jing, Q. (2014). The zebrafish Tie2 signaling controls tip cell behaviors and acts synergistically with Vegf pathway in developmental angiogenesis. *Acta Biochim. Biophys. Sin. (Shanghai)* **46**, 641-646. doi:10.1093/abbs/gmu055
- Limaye, N., Wouters, V., Uebelhoefer, M., Tuominen, M., Wirkkala, R., Mulliken, J. B., Eklund, L., Boon, L. M. and Vikkula, M. (2009). Somatic mutations in angiotensin receptor gene TEK cause solitary and multiple sporadic venous malformations. *Nat. Genet.* **41**, 118-124. doi:10.1038/ng.272
- Lyons, M. S., Bell, B., Stainier, D. and Peters, K. G. (1998). Isolation of the zebrafish homologues for the *tie-1* and *tie-2* endothelium-specific receptor tyrosine kinases. *Dev. Dyn.* **212**, 133-140. doi:10.1002/(SICI)1097-0177(199805)212:1<133::AID-AJA12>3.0.CO;2-8
- Ma, Z., Zhu, P., Shi, H., Guo, L., Zhang, Q., Chen, Y., Chen, S., Zhang, Z., Peng, J. and Chen, J. (2019). PTC-bearing mRNA elicits a genetic compensation response via Upf3a and COMPASS components. *Nature* **568**, 259-263. doi:10.1038/s41586-019-1057-y
- Magadum, S., Banerjee, U., Murugan, P., Gangapur, D. and Ravikesavan, R. (2013). Gene duplication as a major force in evolution. *J. Genet.* **92**, 155-161. doi:10.1007/s12041-013-0212-8
- Maisonpierre, P. C., Suri, C., Jones, P. F., Bartunkova, S., Wiegand, S. J., Radziejewski, C., Compton, D., McClain, J., Aldrich, T. H., Papadopoulos, N. et al. (1997). Angiotensin-2, a natural antagonist for Tie2 that disrupts *in vivo* angiogenesis. *Science* **277**, 55-60. doi:10.1126/science.277.5322.55
- Marass, M., Beisaw, A., Gerri, C., Luzzani, F., Fukuda, N., Gunther, S., Kuenne, C., Reischauer, S. and Stainier, D. Y. R. (2019). Genome-wide strategies reveal target genes of Npas4l associated with vascular development in zebrafish. *Development* **146**, dev173427. doi:10.1242/dev.173427
- Marin-Juez, R., Marass, M., Gauvrit, S., Rossi, A., Lai, S. L., Materna, S. C., Black, B. L. and Stainier, D. Y. (2016). Fast revascularization of the injured area is essential to support zebrafish heart regeneration. *Proc. Natl. Acad. Sci. USA* **113**, 11237-11242. doi:10.1073/pnas.1605431113
- Marron, M. B., Hughes, D. P., Edge, M. D., Forder, C. L. and Brindle, N. P. (2000). Evidence for heterotypic interaction between the receptor tyrosine kinases TIE-1 and TIE-2. *J. Biol. Chem.* **275**, 39741-39746. doi:10.1074/jbc.M007189200
- Nguyen, N. T. T., Vincens, P., Roest Crolius, H. and Louis, A. (2018). Genomic 2018: karyotype evolutionary trees and on-the-fly synteny computing. *Nucleic Acids Res.* **46**, D816-D822. doi:10.1093/nar/gkx1003
- Ohno, S. (1970). *Evolution by Gene Duplication*. New York, NY: Springer Verlag.
- Partanen, J., Armstrong, E., Mäkelä, T. P., Korhonen, J., Sandberg, M., Renkonen, R., Knuutila, S., Huebner, K. and Alitalo, K. (1992). A novel endothelial-cell surface-receptor tyrosine kinase with extracellular epidermal growth-factor homology domains. *Mol. Cell. Biol.* **12**, 1698-1707. doi:10.1128/MCB.12.4.1698
- Pham, V. N., Roman, B. L. and Weinstein, B. M. (2001). Isolation and expression analysis of three zebrafish angiotensin genes. *Dev. Dyn.* **221**, 470-474. doi:10.1002/dvdy.1157
- Puri, M. C., Rossant, J., Alitalo, K., Bernstein, A. and Partanen, J. (1995). The receptor tyrosine kinase TIE is required for integrity and survival of vascular endothelial cells. *EMBO J.* **14**, 5884-5891. doi:10.1002/j.1460-2075.1995.tb00276.x
- Puri, M. C., Partanen, J., Rossant, J. and Bernstein, A. (1999). Interaction of the TEK and TIE receptor tyrosine kinases during cardiovascular development. *Development* **126**, 4569-4580.
- Qu, X., Tompkins, J., Batts, L. E., Puri, M. and Baldwin, H. S. (2010). Abnormal embryonic lymphatic vessel development in *Tie1* hypomorphic mice. *Development* **137**, 1285-1295. doi:10.1242/dev.043380
- Rossi, A., Kontarakis, Z., Gerri, C., Nolte, H., Holper, S., Kruger, M. and Stainier, D. Y. R. (2015). Genetic compensation induced by deleterious mutations but not gene knockdowns. *Nature* **524**, 230-+. doi:10.1038/nature14580
- Saharinen, P., Kerkela, K., Ekman, M., Marron, M., Brindle, N., Lee, G. M., Augustin, H., Koh, G. Y. and Alitalo, K. (2005). Multiple angiotensin recombinant proteins activate the Tie1 receptor tyrosine kinase and promote its interaction with Tie2. *J. Cell Biol.* **169**, 239-243. doi:10.1083/jcb.200411105

- Samarut, E., Lissouba, A. and Drapeau, P. (2016). A simplified method for identifying early CRISPR-induced indels in zebrafish embryos using high resolution melting analysis. *BMC Genomics* **17**, 547. doi:10.1186/s12864-016-2881-1
- Sato, T. N., Qin, Y., Kozak, C. A. and Audus, K. L. (1993). *tie-1* and *tie-2* define another class of putative receptor tyrosine kinase genes expressed in early embryonic vascular system. *Proc. Natl Acad. Sci USA* **90**, 9355-9358. doi:10.1073/pnas.90.20.9355
- Sato, T. N., Tozawa, Y., Deutsch, U., Wolburg-Buchholz, K., Fujiwara, Y., Gendron-Maguire, M., Gridley, T., Wolburg, H., Risau, W. and Qin, Y. (1995). Distinct roles of the receptor tyrosine kinases Tie-1 and Tie-2 in blood vessel formation. *Nature* **376**, 70-74. doi:10.1038/376070a0
- Sato, A., Iwama, A., Takakura, N., Nishio, H., Yancopoulos, G. D. and Suda, T. (1998). Characterization of TEK receptor tyrosine kinase and its ligands, Angiopoietins, in human hematopoietic progenitor cells. *Int. Immunol.* **10**, 1217-1227. doi:10.1093/intimm/10.8.1217
- Savant, S., La Porta, S., Budnik, A., Busch, K., Hu, J., Tisch, N., Korn, C., Valls, A. F., Benest, A. V., Terhardt, D. et al. (2015). The orphan receptor Tie1 controls angiogenesis and vascular remodeling by differentially regulating Tie2 in tip and stalk cells. *Cell reports* **12**, 1761-1773. doi:10.1016/j.celrep.2015.08.024
- Schulte-Merker, S. and Stainier, D. Y. (2014). Out with the old, in with the new: reassessing morpholino knockdowns in light of genome editing technology. *Development* **141**, 3103-3104. doi:10.1242/dev.112003
- Seegar, T. C., Eller, B., Tzvetkova-Robeve, D., Kolev, M. V., Henderson, S. C., Nikolov, D. B. and Barton, W. A. (2010). Tie1-Tie2 interactions mediate functional differences between angiopoietin ligands. *Mol. Cell* **37**, 643-655. doi:10.1016/j.molcel.2010.02.007
- Soblet, J., Limaye, N., Uebelhoer, M., Boon, L. M. and Vikkula, M. (2013). Variable somatic *TIE2* mutations in half of sporadic venous malformations. *Mol. Syndromol.* **4**, 179-183. doi:10.1159/000348327
- Souma, T., Tompson, S. W., Thomson, B. R., Siggs, O. M., Kizhatil, K., Yamaguchi, S., Feng, L., Limviphuvadh, V., Whisenhunt, K. N., Maurer-Stroh, S. et al. (2016). Angiopoietin receptor *TEK* mutations underlie primary congenital glaucoma with variable expressivity. *J. Clin. Invest.* **126**, 2575-2587. doi:10.1172/JCI85830
- Stainier, D. Y., Kontarakis, Z. and Rossi, A. (2015). Making sense of anti-sense data. *Dev. Cell* **32**, 7-8. doi:10.1016/j.devcel.2014.12.012
- Stainier, D. Y. R., Raz, E., Lawson, N. D., Ekker, S. C., Burdine, R. D., Eisen, J. S., Ingham, P. W., Schulte-Merker, S., Yelon, D., Weinstein, B. M. et al. (2017). Guidelines for morpholino use in zebrafish. *PLoS Genet.* **13**, e1007000. doi:10.1371/journal.pgen.1007000
- Stamatakis, A. (2014). RAxML version 8: a tool for phylogenetic analysis and post-analysis of large phylogenies. *Bioinformatics* **30**, 1312-1313. doi:10.1093/bioinformatics/btu033
- Stamatakis, A., Hoover, P. and Rougemont, J. (2008). A rapid bootstrap algorithm for the RAxML Web servers. *Syst. Biol.* **57**, 758-771. doi:10.1080/10635150802429642
- Stevens, M. E., Dhillon, J., Miller, C. A., Messier-Solek, C., Majeske, A. J., Zuelke, D., Rast, J. P. and Smith, L. C. (2010). *SpTie1/2* is expressed in coelomocytes, axial organ and embryos of the sea urchin *Strongylocentrotus purpuratus*, and is an orthologue of vertebrate Tie1 and Tie2. *Dev. Comp. Immunol.* **34**, 884-895. doi:10.1016/j.dci.2010.03.010
- Suri, C., Jones, P. F., Patan, S., Bartunkova, S., Maisonpierre, P. C., Davis, S., Sato, T. N. and Yancopoulos, G. D. (1996). Requisite role of Angiopoietin-1, a ligand for the TIE2 receptor, during embryonic angiogenesis. *Cell* **87**, 1171-1180. doi:10.1016/S0092-8674(00)81813-9
- Tait, C. R. and Jones, P. F. (2004). Angiopoietins in tumours: the angiogenic switch. *J. Pathol.* **204**, 1-10. doi:10.1002/path.1618
- Thambyrajah, R., Ucanok, D., Jalali, M., Hough, Y., Wilkinson, R. N., McMahon, K., Moore, C. and Gering, M. (2016). A gene trap transposon eliminates haematopoietic expression of zebrafish *gfi1aa*, but does not interfere with haematopoiesis. *Dev. Biol.* **417**, 25-39. doi:10.1016/j.ydbio.2016.07.010
- Thurston, G. and Daly, C. (2012). The complex role of angiopoietin-2 in the angiopoietin-tie signaling pathway. *Cold Spring Harb. Perspect Med.* **2**, a006550. doi:10.1101/cshperspect.a006550
- Tran, N. V., Tzovaras, B. G. and Ebersberger, I. (2018). PhyloProfile: dynamic visualization and exploration of multi-layered phylogenetic profiles. *Bioinformatics* **34**, 3041-3043. doi:10.1093/bioinformatics/bty225
- Tuladhar, R., Yeu, Y., Tyler Piazza, J., Tan, Z., Rene Clemenceau, J., Wu, X., Barrett, Q., Herbert, J., Mathews, D. H., Kim, J. et al. (2019). CRISPR-Cas9-based mutagenesis frequently provokes on-target mRNA misregulation. *Nat. Commun.* **10**, 4056. doi:10.1038/s41467-019-12028-5
- Valenzuela, D. M., Griffiths, J. A., Rojas, J., Aldrich, T. H., Jones, P. F., Zhou, H., McClain, J., Copeland, N. G., Gilbert, D. J., Jenkins, N. A. et al. (1999). Angiopoietins 3 and 4: diverging gene counterparts in mice and humans. *Proc. Natl. Acad. Sci. USA* **96**, 1904-1909. doi:10.1073/pnas.96.5.1904
- Voskas, D., Jones, N., Van Slyke, P., Sturk, C., Chang, W., Haninec, A., Babichev, Y. O., Tran, J., Master, Z., Chen, S. et al. (2005). A cyclosporine-sensitive psoriasis-like disease produced in *Tie2* transgenic mice. *Am. J. Pathol.* **166**, 843-855. doi:10.1016/S0002-9440(10)62305-X
- Wilkinson, R. N., Elworthy, S., Ingham, P. W. and van Eeden, F. J. (2013). A method for high-throughput PCR-based genotyping of larval zebrafish tail biopsies. *BioTechniques* **55**, 314-316. doi:10.2144/000114116
- Wouters, V., Limaye, N., Uebelhoer, M., Irrthum, A., Boon, L. M., Mulliken, J. B., Enjolras, O., Baselga, E., Berg, J., DompMartin, A. et al. (2010). Hereditary cutaneomucosal venous malformations are caused by *TIE2* mutations with widely variable hyper-phosphorylating effects. *Eur. J. Hum. Genet.* **18**, 414-420. doi:10.1038/ejhg.2009.193
- Yano, M., Iwama, A., Nishio, H., Suda, J., Takada, G. and Suda, T. (1997). Expression and function of murine receptor tyrosine kinases, *TIE* and *TEK*, in hematopoietic stem cells. *Blood* **89**, 4317-4326. doi:10.1182/blood.V89.12.4317
- Ye, K., Li, J., Li, X., Chang, S. and Zhang, Z. (2018). Ang1/Tie2 induces cell proliferation and migration in human papillary thyroid carcinoma via the PI3K/AKT pathway. *Oncol. Letters* **15**, 1313-1318. doi:10.3892/ol.2017.7367

A *bns347*

(AGCTGCCGTTGGGCTTCAG>GAAACCACTC)
K1042R; L1043N; P1044_G1046del; F1047H; R1048S

Variant	PROVEAN Score	Prediction (Cutoff= -2.5)
K1042R	-1.437	Neutral
L1043N	-5.653	Deleterious
P1044_G1046del	-17.370	Deleterious
F1047H	-0.475	Neutral
R1048S	-5.008	Deleterious

B DNA sequence

```

WT      GAGGAACGCCGTACTGCGGGATGACCTGCGCTGAACTCTATGAGAAGCTGCCGTTGGGCT 60
      |||
bns347 GAGGAACGCCGTACTGCGGGATGACCTGCGCTGAACTCTATGAGA-GAAACCACTCG--- 56

WT      TCAGGCTGGAGAAACCACTGAACT 84
      |||
bns347 -----CTGGAGAAACCACTGAACT 75

```

C Protein sequence

```

WT      NVLVGENFVAKIADFGLSRGQEVYVKKTMGRLPVRWMAIESLNYSVYTTNSDVWSYGVLL 1019
bns347 NVLVGENFVAKIADFGLSRGQEVYVKKTMGRLPVRWMAIESLNYSVYTTNSDVWSYGVLL 1019
      *****

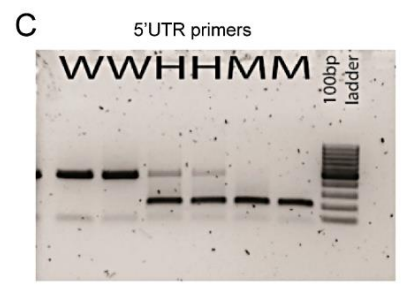
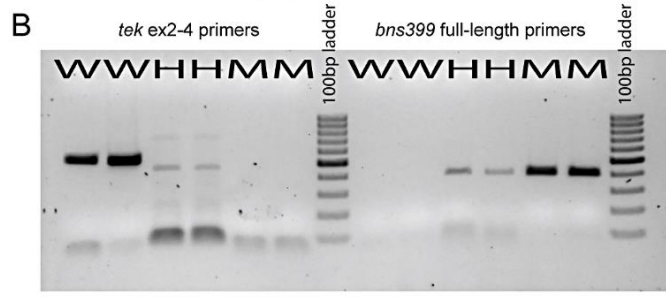
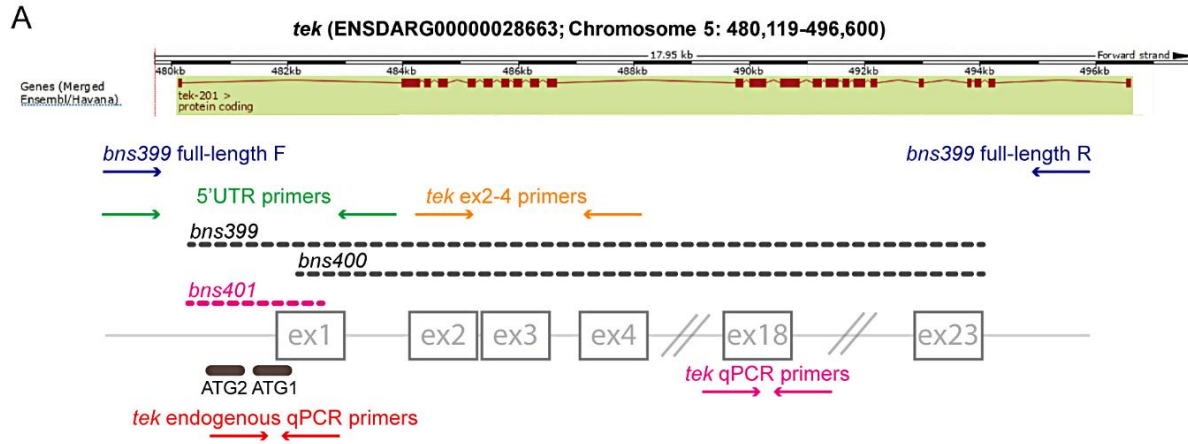
WT      WEVVS LGGTPYCGMTCAELEYE KLPLGFRLEKPLNCDDEVYELMQQCWREKPFERPSFSQI 1079
bns347 WEVVS LGGTPYCGMTCAELEYE RN---HSLEKPLNCDDEVYELMQQCWREKPFERPSFSQI 1076
      *****

WT      LLSLGRMLEERKTYVNTTLYEKFTYAGIDCSAEEAG 1115
bns347 LLSLGRMLEERKTYVNTTLYEKFTYAGIDCSAEEAG 1112
      *****

```

Figure S1. *tek^{bns347}* in-frame deletion is predicted to severely impair Tek function.

(A) The *tek^{bns347}* allele contains a 19 bp deletion (AGCTGCCGTTGGGCTTCAG) and a 10 bp insertion (GAAACCACTC) in exon 21, resulting in K1042R, L1043N, P1044_G1046 deletion, F1047H and R1048S in the TK domain; PROVEAN analysis indicates that this lesion is overall deleterious. (B) *tek^{bns347}* in-frame deletion as revealed by Sanger sequencing (partial sequence of exon 21 shown). (C) Amino acid sequence alignment of WT and Tek^{bns347} proteins.



D

WT CCCTGCAGGCTGGGTTACAGGAGGTCG . . . GAGGAGGCCGGCTGATGCGCTGCCGCAAT

bns399 CCCTGCAGGCTGGGT-----GATGCGCTGCCGCAAT

***** ← 16733 bp deletion → *****

E

WT CCTGCAGGCTGGGTTACAGGAGGTCG . . . CTGCTCTGCTGCTGCTCGGCTGCTGGA

bns401 CCTGCAGGCTGGGT-----TGCTCGGCTGCTGGA

***** ← 261 bp deletion → *****

F *bns401*

Variant	PROVEAN Score	Prediction (Cutoff= -2.5)
M1_W16del	-2.067	Neutral

G Protein sequence

WT MCLLDSC TALLLLGCWMSGSAVRISDVTLVNPDPVVSPLTAPSLLCVSSDWSSGGSVLAL 60

bns401 -----MSGSAVRISDVTLVNPDPVVSPLTAPSLLCVSSDWSSGGSVLAL 44

WT GQEFPRPQGSVLALGQEFPHTEPRPHPAAATVTWSSRS HAFGAFYCQIRNSTGRKIITYK 120

bns401 GQEFPRPQGSVLALGQEFPHTEPRPHPAAATVTWSSRS HAFGAFYCQIRNSTGRKIITYK 104

Figure S2. Genotyping the *tek*^{bns399} RNA-less allele and the *tek*^{bns401} 5'UTR deletion allele, and location of relevant primers.

(A) *tek* locus based on Ensembl annotation and schematic positioning of the genotyping and RT-PCR primers (arrows), the MOs (bold solid lines), and the deletions (dashed lines). (B) Genotyping the *tek*^{bns399} RNA-less allele with different PCR primer sets to identify WT and mutant bands. (C) Genotyping the *tek*^{bns401} 5'UTR deletion allele by PCR. (D) Deletion in the *tek*^{bns399} RNA-less allele as revealed by Sanger sequencing. (E) Deletion in the *tek*^{bns401} allele as revealed by Sanger sequencing. (F) The *tek*^{bns401} allele contains a 261 bp deletion, resulting in M1_W16 deletion; PROVEAN analysis indicates that this lesion is overall neutral. (G) Amino acid sequence alignment of WT and Tek^{bns401} proteins.

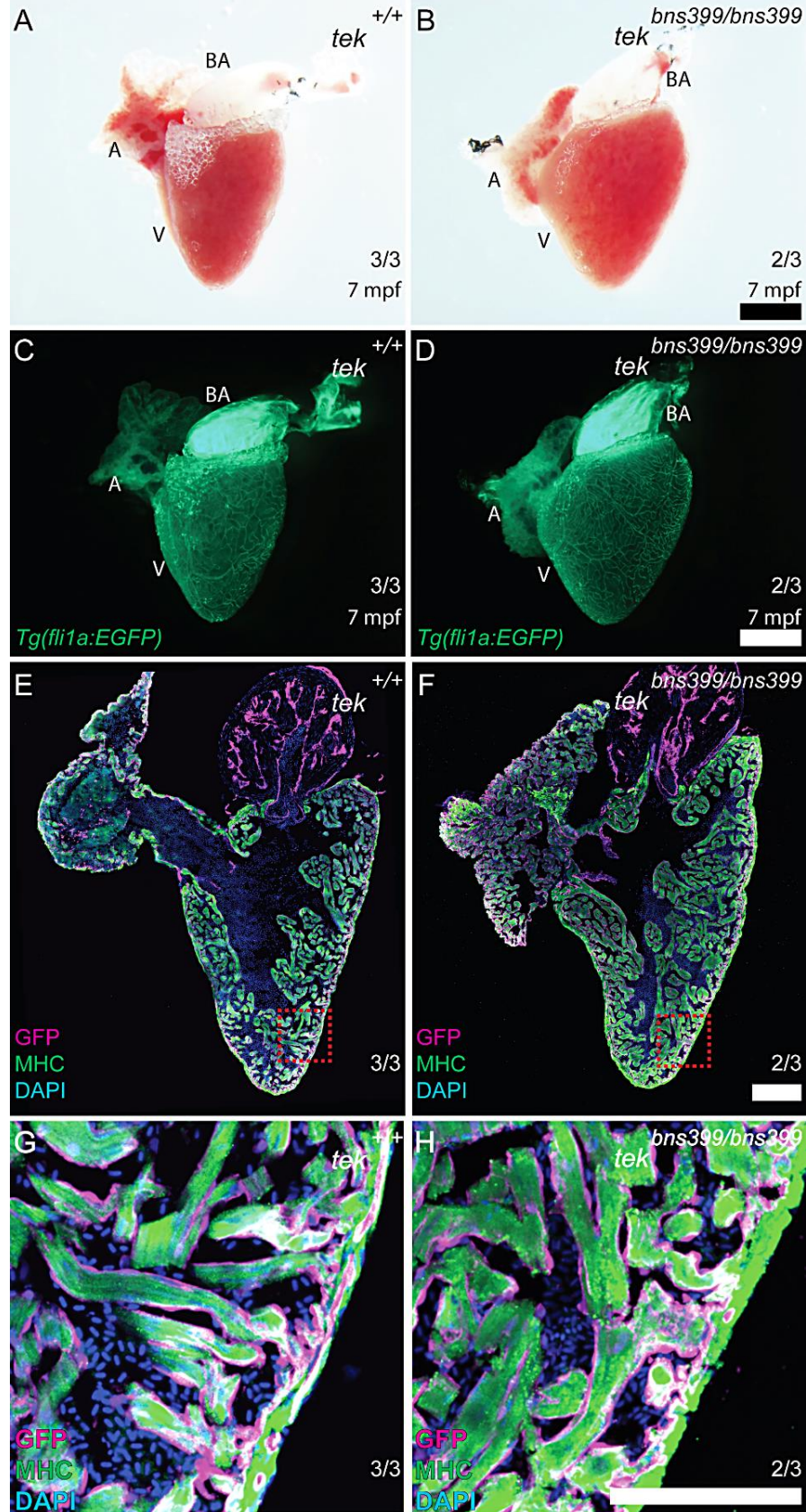


Figure S3. No obvious phenotypes in adult hearts of *tek^{bns399}* RNA-less mutants.

(A, B) Brightfield images of dissected hearts from 7 mpf *+/+* siblings (A) and *tek^{bns399/bns399}* animals (B). (C, D) Fluorescent images of coronary vessels in dissected hearts from 7 mpf *Tg(fli1a:EGFP) +/+* siblings (C) and *tek^{bns399/bns399}* animals (D). Scale bars: 500 μ m. (E-H) Sections of dissected hearts from 7 mpf *+/+* siblings (E, G) and *tek^{bns399/bns399}* animals (F, H). Endothelial cells immunostained with anti-GFP (magenta), cardiomyocytes with anti-MHC antibody (green), and nuclei counterstained with DAPI (blue). (G, H) Magnified figures of red-boxed areas in panels E and F, respectively. Scale bars: 200 μ m.

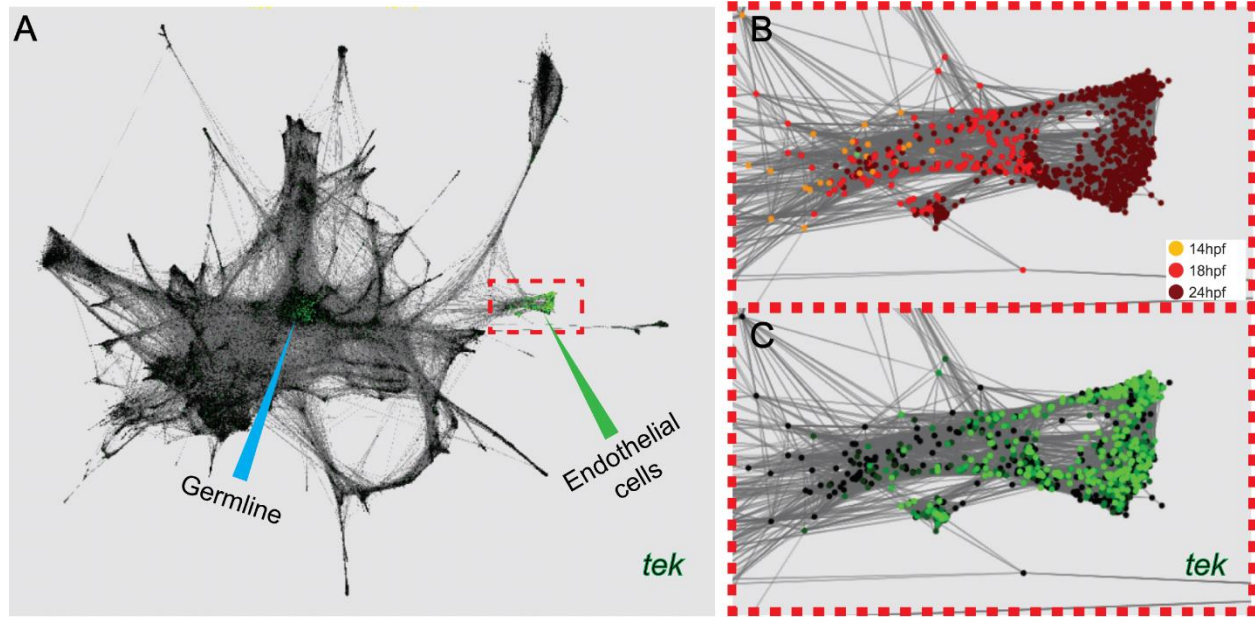


Figure S4. Embryonic expression of *tek* is highly enriched in endothelial cells.

(A) Overview of zebrafish *tek* expression in the single cell RNA-Seq dataset from the Klein lab (https://kleintools.hms.harvard.edu/paper_websites/wagner_zebrafish_timecourse2018/mainpage.html). *tek* positive cells are highlighted in green. (B) Magnified figure of the red boxed endothelial cell group from panel A, showing an overview of the zebrafish single cell RNA-Seq data at different time points. (C) *tek* expression is endothelial cell enriched.

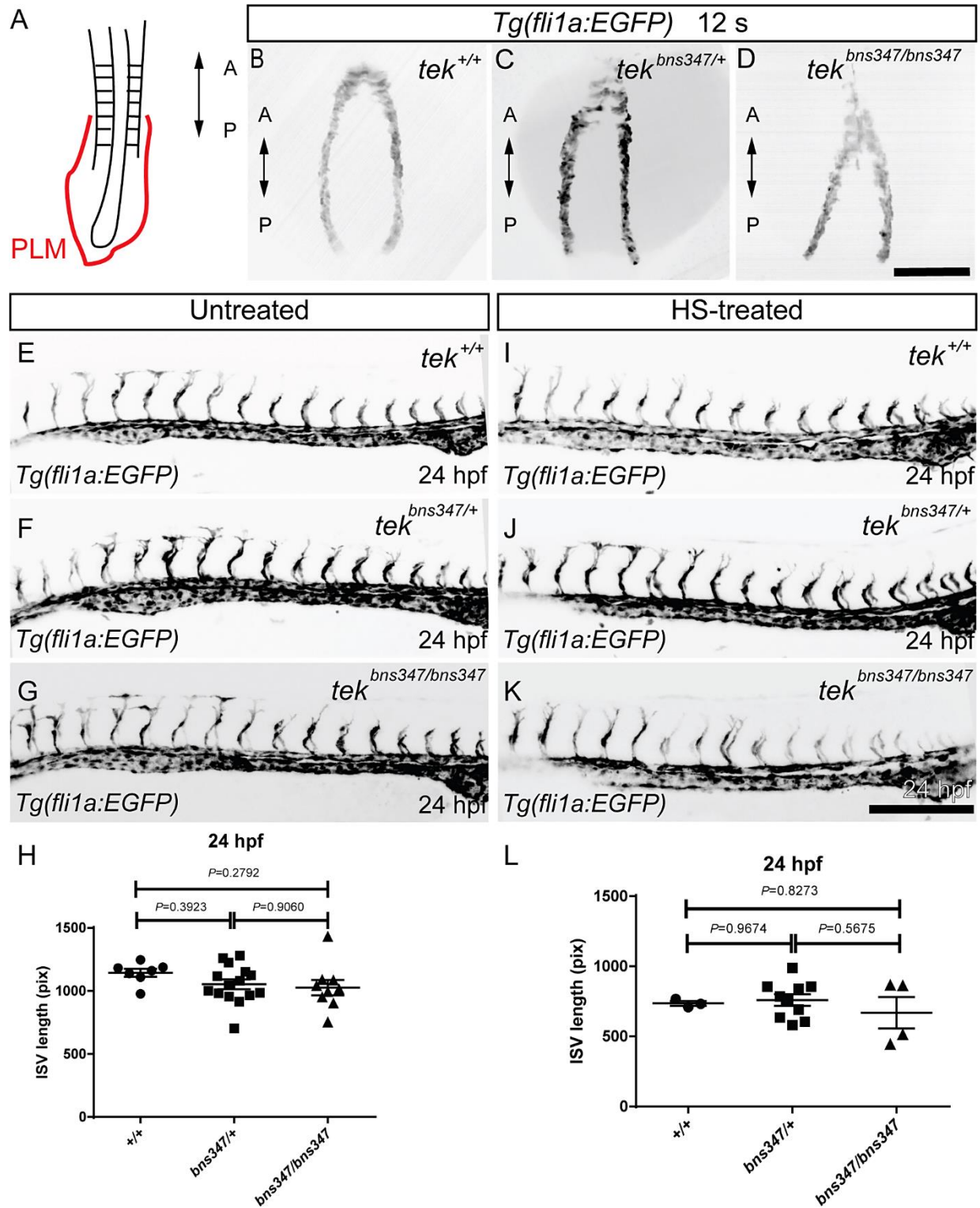


Figure S5. No obvious phenotypes in *tek*^{bns347} in-frame deletion mutants at early or late stages.

(A) Schematic representation of the posterior lateral plate mesoderm (PLM). (B-D) Dorsal views of the PLM in *tek*^{bns347/+} incrossed embryos at the 12 somite-stage. (E-G) Lateral views of trunk vessels in 24 hpf *tek*^{bns347/+} incrossed embryos. (H) Total length of 14 ISVs above the yolk extension in 24 hpf *tek*^{bns347/+} incrossed embryos. (I-K) Lateral views of trunk vessels in 24 hpf *tek*^{bns347/+} incrossed embryos heat-shocked (HS) at 10 and 22 hpf for 1 hour. (L) Total length of 14 ISVs above the yolk extension in 24 hpf *tek*^{bns347/+} incrossed embryos heat-shocked at 10 and 22 hpf for 1 hour. In panels H and L, error bars represent means \pm SD (by one-way analysis of variance (ANOVA) followed by Tukey's HSD test). Scale bars: 200 μ m.

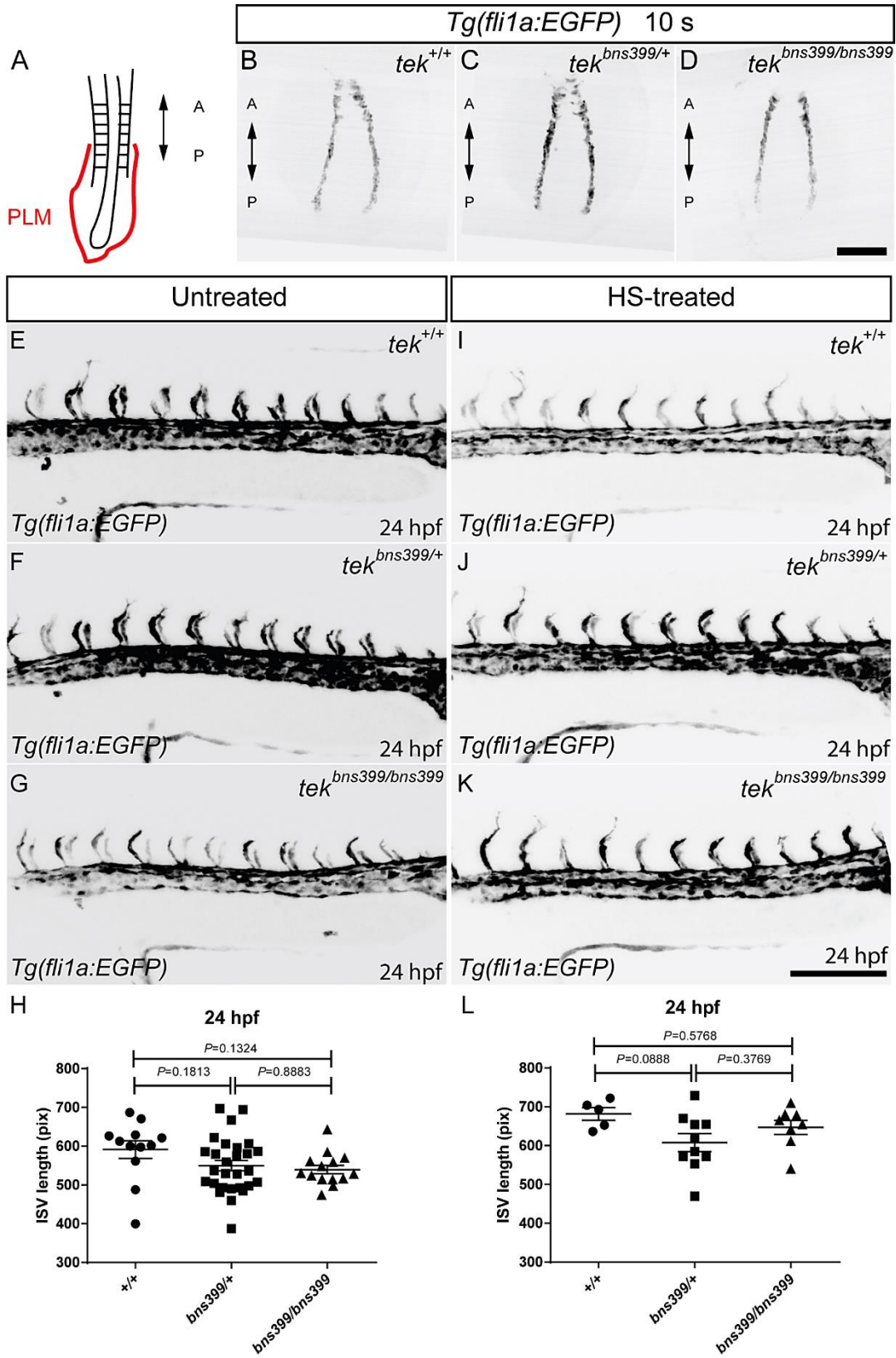


Figure S6. No obvious phenotypes in *tek^{bns399}* RNA-less mutants at early or late stages.

(A) Schematic representation of the posterior lateral plate mesoderm (PLM). (B-D) Dorsal views of the PLM in *tek^{bns399/+}* incrossed embryos at the 10 somite-stage. (E-G) Lateral views of trunk vessels in 24 hpf *tek^{bns399/+}* incrossed embryos. (H) Total length of 10 ISVs above the yolk extension in 24 hpf *tek^{bns399/+}* incrossed embryos. (I-K) Lateral views of trunk vessels in 24 hpf *tek^{bns399/+}* incrossed embryos heat-shocked (HS) at 10 and 22 hpf for 1 hour. (L) Total length of 10 ISVs above the yolk extension in 24 hpf *tek^{bns399/+}* incrossed embryos heat-shocked at 10 and 22 hpf for 1 hour. In panels H and L, error bars represent means \pm SD (by one-way analysis of variance (ANOVA) followed by Tukey's HSD test). Scale bars: 200 μ m.

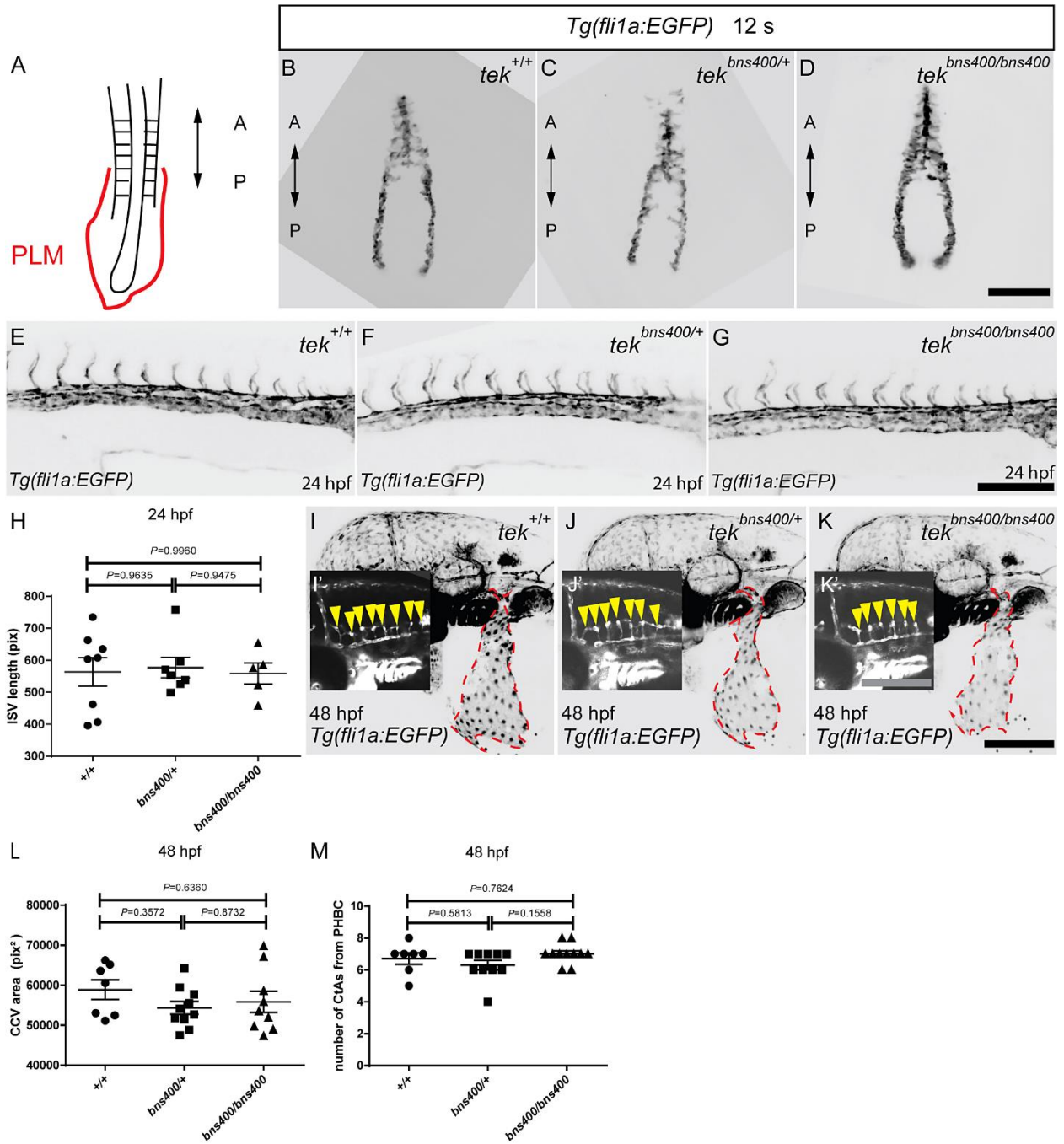


Figure S7. No obvious phenotypes in *tek^{bns400}* RNA-less mutants at early or late stages.

(A) Schematic representation of the posterior lateral plate mesoderm (PLM). (B-D) Dorsal views of the PLM in *tek^{bns400/+}* incrossed embryos at the 12 somite-stage. (E-G) Lateral views of trunk vessels in 24 hpf *tek^{bns400/+}* incrossed embryos. (H) Total length of 10 ISVs above the yolk extension in 24 hpf *tek^{bns400/+}* incrossed embryos. (I-K) Lateral views of the head vasculature in 48 hpf *tek^{bns400/+}* incrossed embryos. Red dashed lines outline the CCV. (I'-K') Lateral views of the head vessels in 48 hpf *tek^{bns400/+}* incrossed embryos. Yellow arrowheads point to CtAs. (L) CCV area in 48 hpf *tek^{bns400/+}* incrossed embryos. (M) CtA numbers in *tek^{bns400/+}* incrossed embryos at 48 hpf. CtA: Central Artery; CCV: Common Cardinal Vein. In panels H, L and M, error bars represent means \pm SD (by one-way analysis of variance (ANOVA) followed by Tukey's HSD test). Scale bars: 200 μ m.

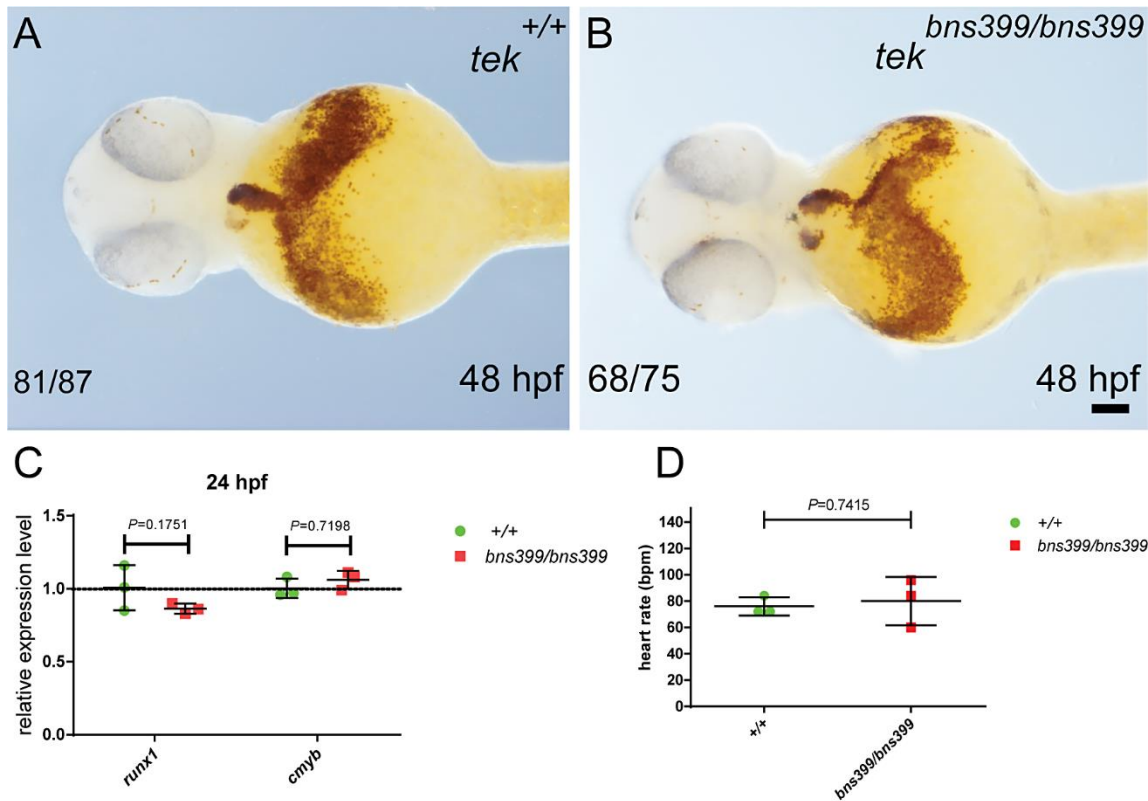


Figure S8. No obvious blood-related phenotypes in tek^{bns399} RNA-less mutants.

(A, B) Ventral views of erythrocytes in 48 hpf $+/+$ siblings (A) and $tek^{bns399/bns399}$ embryos (B) stained with O-Dianisidine. (C) *runx1* and *cmyb* mRNA levels in $tek^{bns399/bns399}$ mutants when compared to their corresponding $+/+$ siblings at 24 hpf. (D) Heart rate in 7 mpf $tek^{bns399/bns399}$ mutants when compared to their corresponding $+/+$ siblings. Scale bar: 100 μ m.

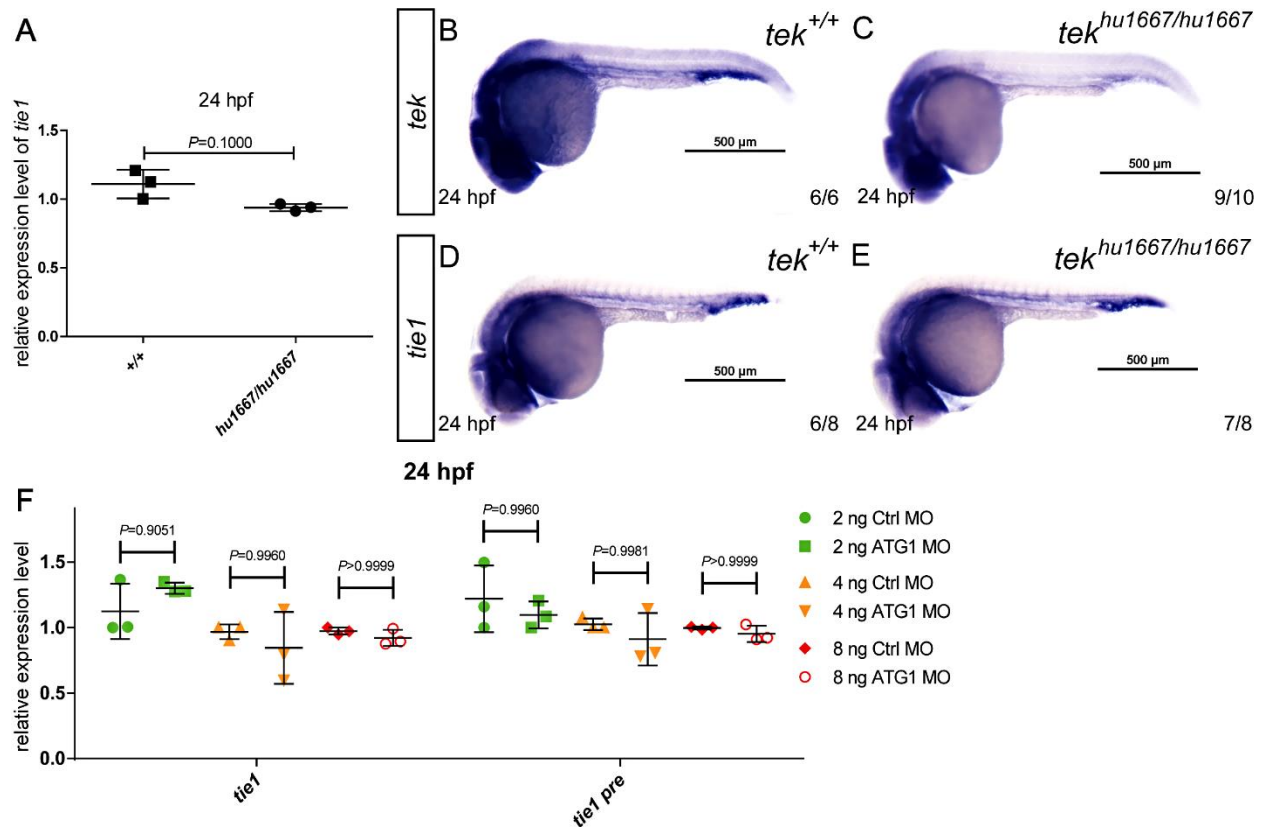


Figure S9. *tie1* does not appear to compensate for the loss of Tek function.

(A) *tek* mRNA levels in $tek^{hu1667/hu1667}$ mutants when compared to their $+/+$ siblings at 24 hpf. (B-E) Expression of *tek* (B, C) and *tie1* (D, E), as detected by wholemount *in situ* hybridization, in 24 hpf $tek^{hu1667/+}$ increased embryos. (F) *tie1* mRNA and pre-mRNA levels in *tek* ATG1 morphants when compared to control morphants at 24 hpf. In panel A, error bars represent means \pm SD (by Mann-Whitney *U* test). In panel F, error bars represent means \pm SD (by Two-way analysis of variance (ANOVA) followed by Tukey's HSD test). Scale bars: 500 μ m.

Vertebrates

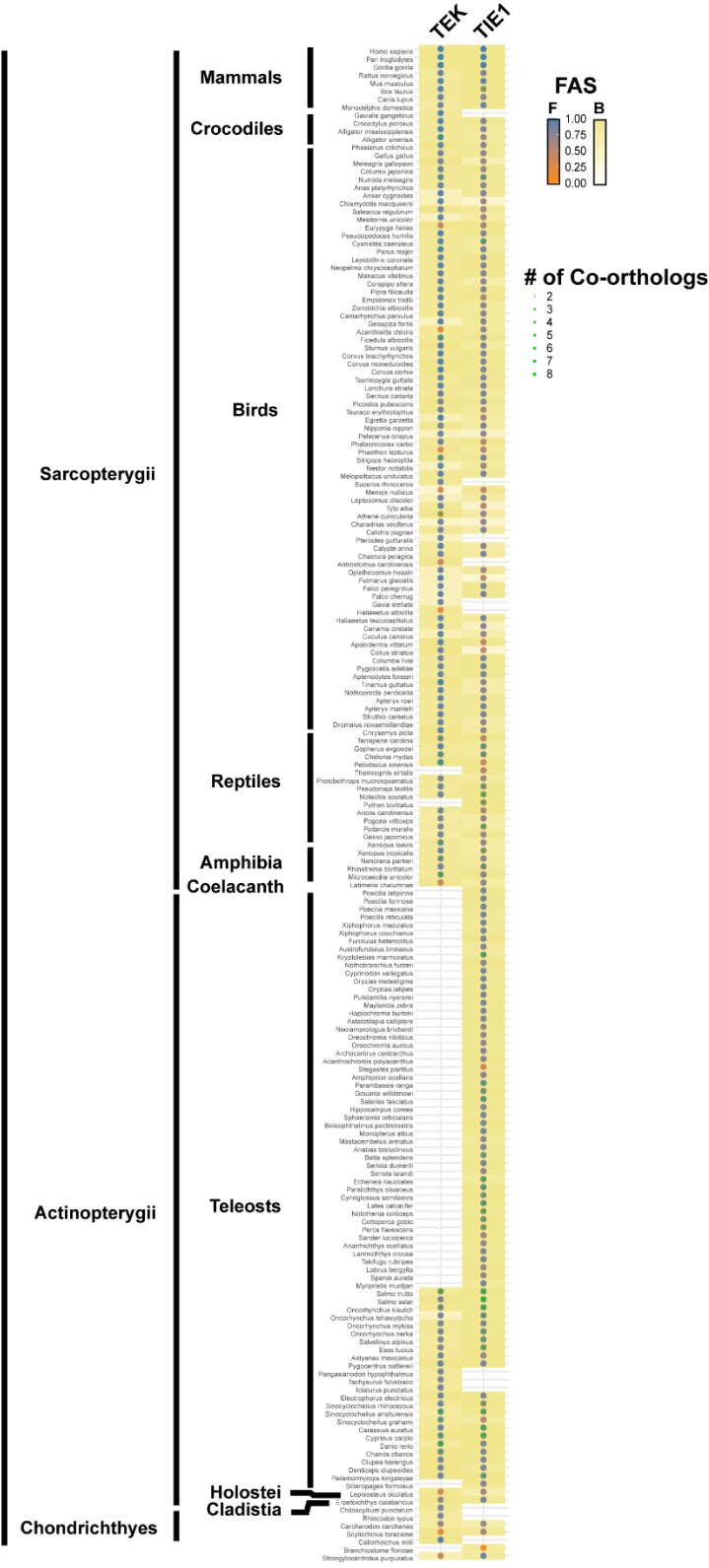


Figure S10. Phylogenetic profile of TEK and TIE1 on a species level resolution.

A dot represents the detection of an ortholog to human TEK or TIE1 in the corresponding species. Inner green circles indicate the presence of co-orthologs to the human protein where the size of the circle represents the number of co-orthologs. Dot colour and cell colour represent the feature architecture similarity score between two orthologs using the human protein (dot colour) and the ortholog (cell colour) as reference, respectively. The data underlying this plot are available in supplementary file 2.

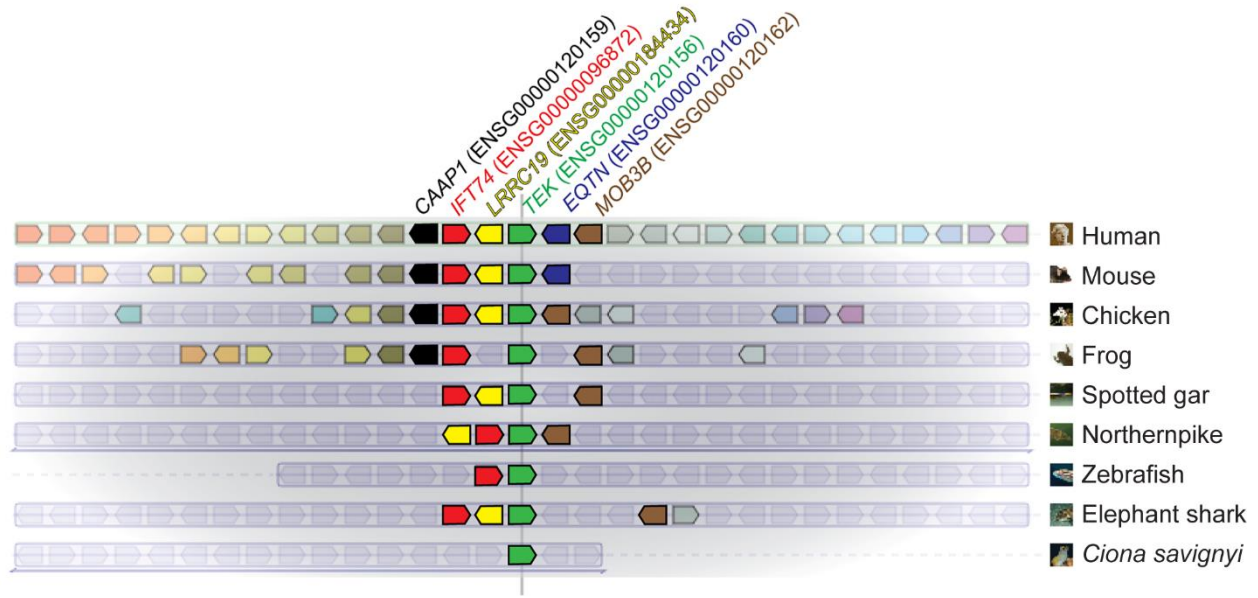


Figure S11. Gene order around the *Tek* locus in various species.

PhyloView representation of *TEK* in the human genome and its orthologs in other genomes. *TEK* and its orthologs are positioned in the centre aligned with their neighbouring genes in various genomes. Genes of the same colour represent orthologs. The location of *ift74* (marked in red), as a direct upstream neighbour of *tek* in the zebrafish genome, is widely conserved amongst different vertebrate species.

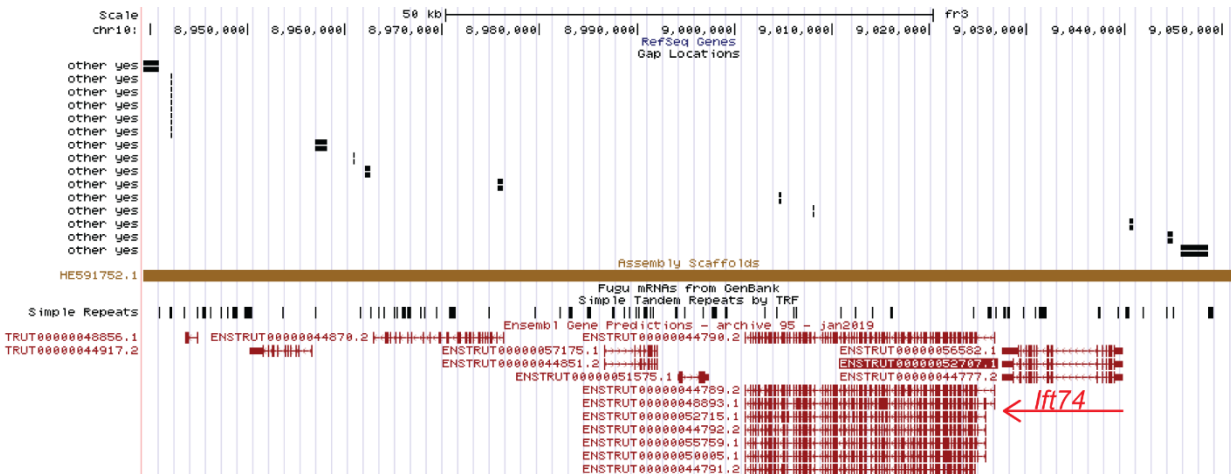


Figure S12. Genomic region distal to *ift74* in *fugu*.

ift74 is located to the far right of the plot (ENSTRUT0000052707). Downstream of *ift74*, in the direction of its transcription, five additional genes are annotated, none of which resembles a *Tek*-like gene. Only very few and small assembly gaps exist in this region (black blocks), and most of them overlap with other annotated genes. These data suggest that the absence of *Tek* in this species cannot be explained by an assembly artefact. The data shown represent the UCSC Genome Browser on the *Fugu* Oct. 2011 (FUGU5/fr3) Assembly (<https://genome.ucsc.edu>).

Vertebrates

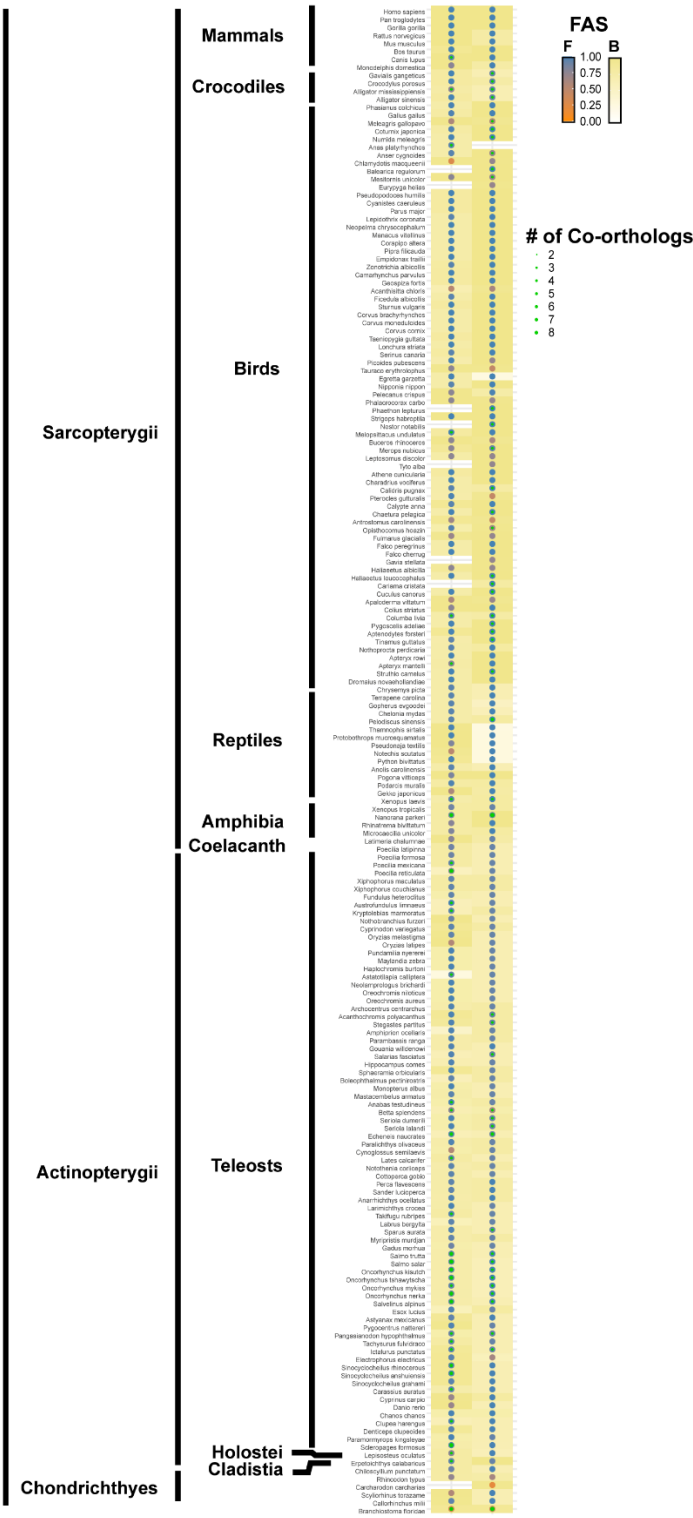
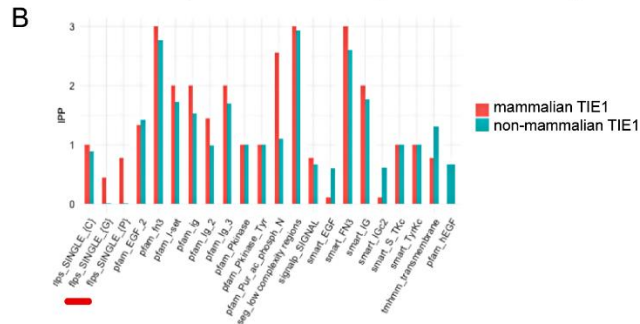
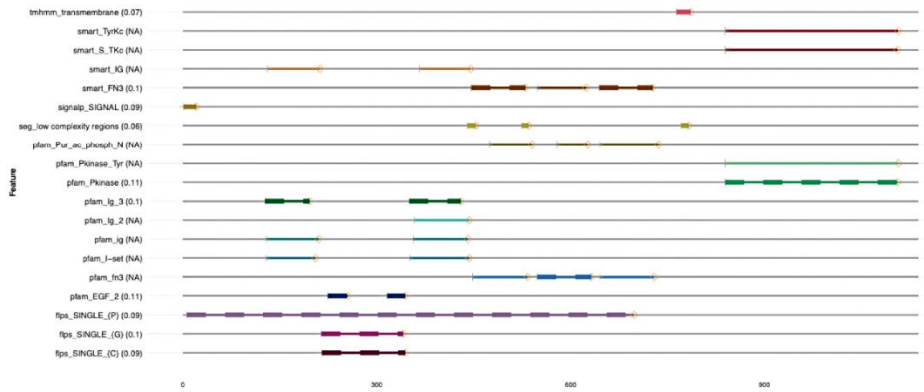


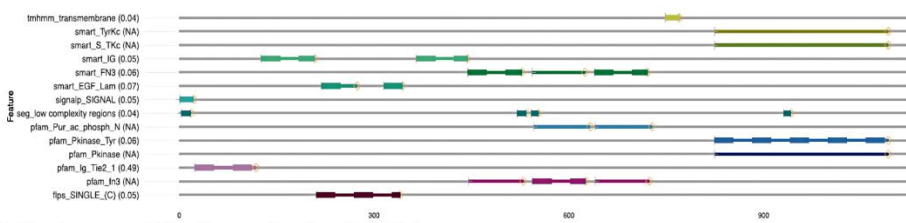
Figure S13. Phylogenetic profile of Angiopoietin-1 and Angiopoietin-2 on a species level resolution.

A dot represents the detection of an ortholog to human Angiopoietin-1 or Angiopoietin-2 in the corresponding species. Inner green circles indicate the presence of co-orthologs to the human protein where the size of the circle represents the number of co-orthologs. Dot colour and cell colour represent the feature architecture similarity score between two orthologs using the human protein (dot colour) and the ortholog (cell colour) as reference, respectively. The data underlying this plot are available in supplementary file 2.

A Feature architecture of human TIE1



C Feature architecture of human TEK



D Feature architecture of zebrafish Tek

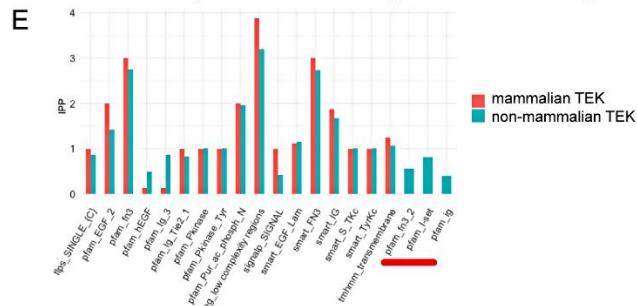
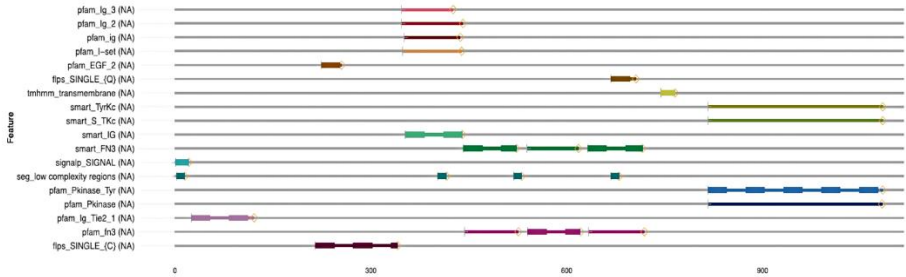


Figure S14. Protein feature architecture of the TIE family receptors has changed on the mammalian lineage.

(A) Schematic representation of human TIE1 protein feature architecture. (B) Comparison of protein feature architecture between mammalian and non-mammalian TIE1 orthologs reveals that mammalian TIE1 harbours a proline and glycine-rich N-terminus (corresponding features are highlighted with red lines). (C) Schematic representation of human TEK protein feature architecture. (D) Schematic representation of zebrafish Tek protein feature architecture. (E) Comparison of feature architecture between mammalian and non-mammalian TEK orthologs reveals that mammalian TEK has a unique Ig2 domain architecture (corresponding features are highlighted with red lines). In panels A, C and D, the numbers next to each protein feature represent the weight of the respective features during scoring of the feature architecture similarity. In the case of overlapping PFAM and SMART domains, we selected the domain that maximizes the similarity score between the two proteins; the weight of the corresponding features was set to 'N.A.'. IPP: Feature instances per protein.

Table S1.

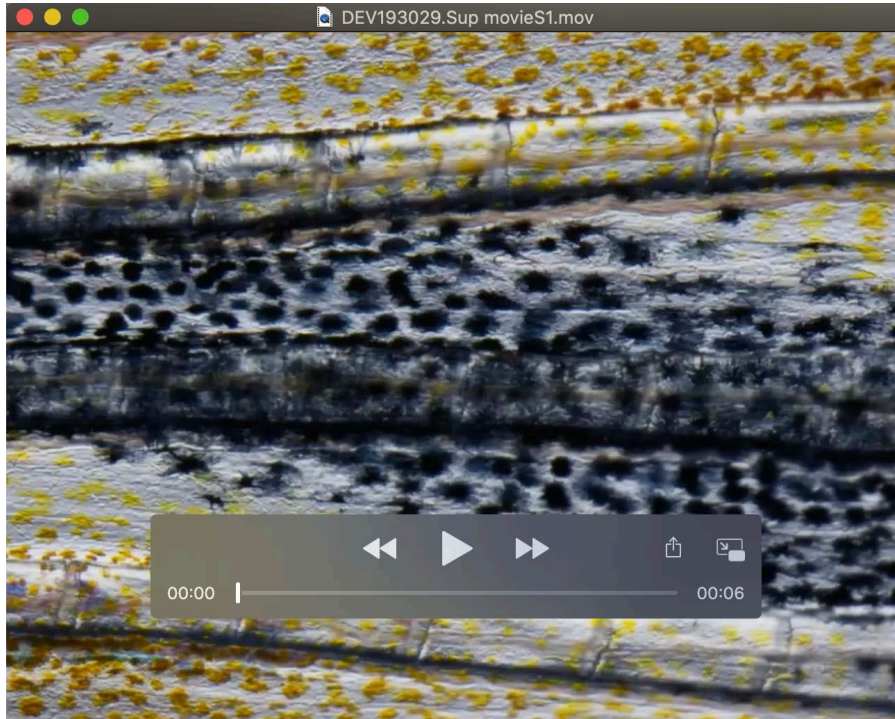
[Click here to Download Table S1](#)

Table S2.

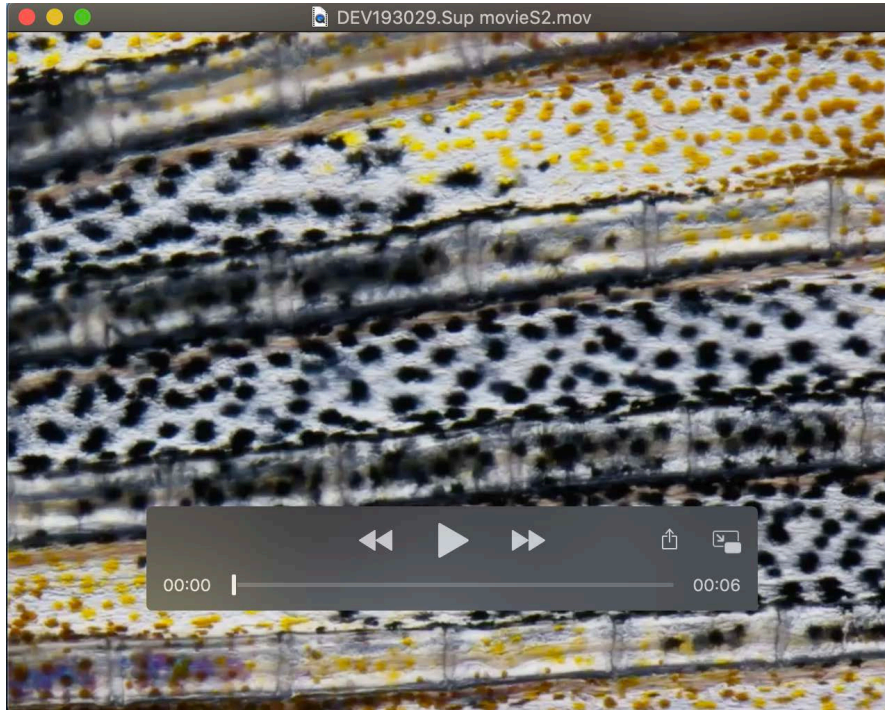
[Click here to Download Table S2](#)

Table S3.

[Click here to Download Table S3](#)



Movie 1. fin blood flow in WT



Movie 2. fin blood flow in mutant



Movie 3. heartbeat in WT



Movie 4. heartbeat in mutant